Dean vortices-induced enhancement of mass transfer through an interface separating two immiscible liquids

A. Yu. Gelfgat
Department of Fluid Mechanics and Heat Transfer, Faculty of Engineering, Tel-Aviv University, Ramat Aviv 69978, Israel

A. L. Yarin and P. Z. Bar-Yoseph
Faculty of Mechanical Engineering, Technion–Israel Institute of Technology, Haifa, 32000, Israel

Two-fluid Dean vortex flow in a coiled pipe with vanishing torsion, and its effect on the mass transfer through the liquid–liquid interface of two immiscible fluids are studied numerically. The liquids are stratified by gravity, with the denser one occupying the lower part of the pipe. The Navier–Stokes equations in both fluid layers are solved numerically by the finite volume method. The results reveal a detailed structure of the transverse flow (the Dean vortices) in coiled pipes with the dimensionless curvature 0.1. Both cocurrent and countercurrent axial flows in the fluid layers are considered. Using the flow fields predicted, the mass transfer equation is solved. It is shown that the mass transfer of a passive scalar (say, a protein with the Schmidt number of the order of 10^3) through the interface can be significantly enhanced by the Dean vortices, so that the mass transfer rate can be increased by three to four times. This makes the Dean vortex flow an effective tool for mass transfer enhancement at the liquid–liquid interface. It is shown that the Dean flow provides a stronger mixing than the Taylor–Couette flow. It is also shown that there exists an optimal axial flow rate in terms of this enhancement. The optimal flow corresponds to the value of the Dean number of about 180. In the countercurrent flow case the Dean vortices can split, which has a negative effect on the mass transfer enhancement. Both the cocurrent and countercurrent axial flows yield a similar enhancement effect on the interfacial mass transfer rate. The problem is related to the search for novel bioseparator devices. © *2003 American Institute of Physics.* [DOI: 10.1063/1.1532732]

I. INTRODUCTION

In the present study, the effect of a two-fluid Dean vortical flow on mass transfer through an interface separating two immiscible liquids is examined. The study is motivated by the problem of extraction of admixtures having extremely low diffusion coefficients, e.g., proteins. Since purely diffusional mass transfer of such admixtures is too slow and has to be enhanced, mixing by vortical flows is called for.[1] In such flows the vortices inside each fluid transport the admixture toward the interface, which yields steeper concentration gradients there. As a result, the mass fluxes through the interface increase and the mass transfer intensifies, even though the diffusion coefficient remains small. The first experimental attempt in this direction was made in Ref. 2, with two-fluid Taylor–Couette vortical flow used in a specially designed bioseparator/bioreactor. This configuration was further studied theoretically and numerically in Ref. 3, where the effect of the Taylor vortices and of the axial throughflow on the mass transfer rates was investigated. Practical application of the two-fluid Taylor–Couette apparatus was found to be problematic because the contact of the rapidly rotating cylindrical boundaries (e.g., in the experiments[2] the rotation rate exceeded 10 rev/s) with the stationary closed ends leads to instability of the liquid–liquid interface. This instability was also observed numerically by the present group. It was compared to the experimental results obtained using the de-

vice of Refs. 1 and 2, and the results will be published in a separate paper. Search for configurations in which the vortical flow can be generated without motion of the boundaries, and which can be implemented in novel bioseparators/bioreactors, led to study of stationary dc streaming generated in emulsions,[4] thin channels with capillary waves,[5] and of natural-convection flow in two-layer horizontal annuli.

The Dean vortices arising in coiled pipe single-liquid flows are known as an effective means for heat and mass transfer enhancement (see Refs. 6–11 and references therein). In particular, Refs. 6 and 7 were motivated by the need to prevent buildup of retained solute concentration near a membrane in a reverse osmosis system. In these works it was shown that the concentration buildup, known as concentration polarization, can be significantly reduced if solutions are supplied through curved channels, where the Dean vortices arise. The Dean vortices effectively mix the retained solute and this results in depolarization and a significant increase in the transmembrane flux. In Refs. 6 and 7, as well as in the previous works of that group, direct numerical simulation was used to calculate the velocity fields in curved channels and pipes with single fluid flowing under different conditions (different Reynolds numbers, channel curvature, etc.). Comparison with the experimental data obtained by means of magnetic resonance flow imaging showed that the numerical results are capable of reproducing the details of the secondary flows (the Dean vortices) rather accurately in-
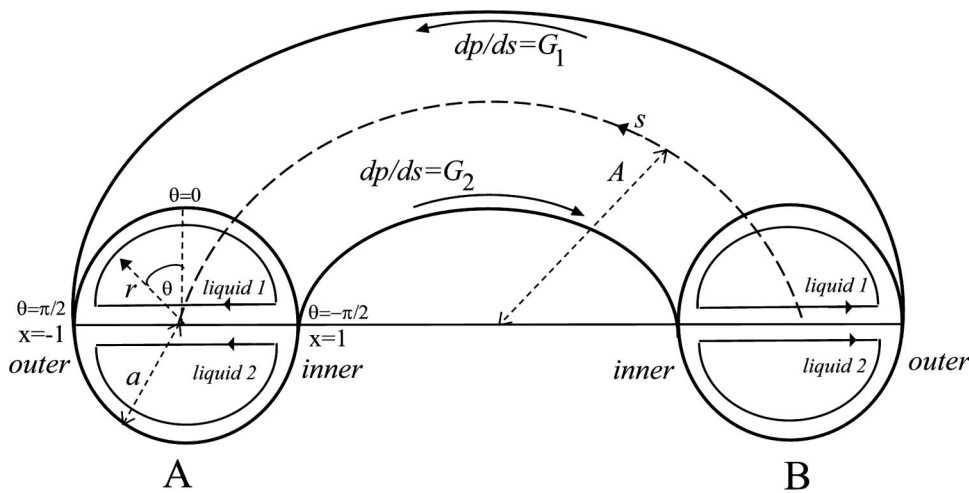
FIG. 1. Sketch of the problem.

cluding bifurcations of the additional vortices. Based on the numerically generated velocity fields, the concentration field was calculated numerically in Ref. 7, where it was shown that concentration polarization in curved channels can be significantly inhibited by the Dean vortices as compared to that in flat channels (where the secondary vortices do not arise).

The present work deals in the same context, with mass transfer enhancement by the Dean vortices developing in coiled pipes of circular cross section filled by two liquid layers formed by immiscible fluids. The flow is driven by the pressure gradient, which acts along the pipe centerline and can be the same or different in the fluid layers. The Dean vortices, driven by the excessive centrifugal force, develop in each layer. It is assumed that each fluid layer occupies half of the pipe cross section. For a preliminary insight into the possibility of the mass transfer enhancement, we consider a helical pipe with vanishing torsion,[12,13] so that the flow region reduces to a circular pipe coiled in a circle. The two immiscible liquid layers, stratified by gravity, then occupy the lower and upper parts of the torus so that the interface coincides with the symmetry plane. To the best of our knowledge, such two-liquid flow in a coiled pipe has never been considered before. The emergence of Dean vortices in two-fluid Dean flows, which are the counterpart of the classical Dean problem,[14] was demonstrated in Ref. 15, where channel flow was considered. In the present work novel results on two-fluid flow in coiled pipes (the counterpart of the single-fluid flow of Ref. 16) are discussed. In particular, the patterns of the Dean vortices, as well as the quantitative results on the Dean-vortex-enhancement of the mass transfer through the liquid–liquid interface are revealed.

Section II presents the problem formulation and briefly discusses the numerical technique employed. The results are presented and discussed in Sec. III. Conclusions are drawn in Sec. IV.

II. FORMULATION OF PROBLEM AND NUMERICAL TECHNIQUE

To estimate the effect of the Dean vortices on the mass transfer we follow Ref. 13 and consider a helical pipe with vanishing torsion. Thus, we consider the flow in a pipe with circular cross section of radius a, coiled in a circle of radius A. Following the classical Dean formulation,[16] it can be interpreted as flow in a torus with centerline of radius A and cross section of radius a. The flow region is shown schematically in Fig. 1. The upper and lower halves of the torus are filled with two immiscible liquids, denoted 1 and 2. The problem is considered in the coordinate system (r,θ,s), where (r,θ) are the polar coordinates in the cross section of the pipe, and s is the arclength along the centerline of the torus.[17] It is assumed that the flow is driven by constant pressure gradients G_1 and G_2 in the s direction, which can be different in each of the liquid layers. In the case of unequal pressures and pressure gradients in the layers, the interface is assumed to be slightly inclined and, as a result, stabilized by gravity. It is also assumed that the liquid–liquid interface is nondeformable and located approximately at the plane $\theta = \pm \pi/2$ and that the mass transfer does not affect the flow. Denoting all the variables and parameters related to liquids 1 and 2 by the corresponding subscripts, the flow in each layer is described by the dimensionless momentum and continuity equations

$$\frac{\partial \mathbf{v}_1}{\partial t} + (\mathbf{v}_1 \cdot \nabla)\mathbf{v}_1 = -\mathbf{e}_s - \nabla p_1 + \frac{1}{R}\Delta \mathbf{v}_1, \tag{1}$$

$$\nabla \cdot \mathbf{v}_1 = 0, \tag{2}$$

$$\frac{\partial \mathbf{v}_2}{\partial t} + (\mathbf{v}_2 \cdot \nabla)\mathbf{v}_2 = -\frac{G_{21}}{\rho_{21}}\mathbf{e}_s - \frac{1}{\rho_{21}}\nabla p_2 + \frac{\mu_{21}}{\rho_{21}}\frac{1}{R}\Delta \mathbf{v}_2, \tag{3}$$

$$\nabla \cdot \mathbf{v}_2 = 0. \tag{4}$$

Here $\mathbf{v}_k = (u_k, v_k, w_k)$ is the flow velocity vector, and p_k the pressure $(k=1,2)$; $\mathbf{e}_s$ is the axial unit vector in the pipe. Furthermore, $\rho_{21} = \rho_2/\rho_1$, $\mu_{21} = \mu_2/\mu_1$ and $G_{21} = G_2/G_1$ are the ratios of the densities, dynamic viscosities, and pressure gradients, respectively. The length, time, velocity and pressure in (1)–(4) are rendered dimensionless by a, $(\rho_1 a/G_1)^{1/2}$, $(G_1 a/\rho_1)^{1/2}$, and $G_1 a$, respectively, so that the value of the dimensionless external pressure gradient in layer 1 is reduced to unity. The nondimensional parameter $R = (a/\mu_1)\sqrt{G_1 a \rho_1}$ is thus the analog of the Reynolds number. Details on the momentum and continuity equations in

the chosen coordinate system are given in Appendix A. Note that an additional governing parameter is the dimensionless curvature of the pipe, $\varepsilon = a/A$. Note also that gravity is assumed to be fully offset by the steady-state component of the vertical pressure gradient, whereby both factors are eliminated from Eqs. (1) and (3).

It is emphasized that the above-introduced nondimensional parameter R is a formal ratio of the inertial to viscous forces. On the other hand, it is desirable to introduce also the Reynolds number Re based on the mean flow velocity $\bar{W}_1$ corresponding to the single-layer flow (liquid 1 only) in a straight pipe of radius a. According to the Poiseuille formula $\bar{W}_1 = a^2 G_1/(8\mu_1)$. Hence, $\text{Re} = \rho_1 a \bar{W}_1/\mu_1 = \rho_1 a^3 G_1/(8\mu_1^2)$. The latter shows that $\text{Re} = R^2/8$. Introducing the Dean number as[13] $\text{D} = \sqrt{2\varepsilon}\rho_1 a^3 G_1/\mu_1^2 = 8(2\varepsilon)^{1/2}\text{Re}$, we have $\text{D} = (2\varepsilon)^{1/2} R^2$. The dimensionless group K of Ref. 12 is $K = \text{D}/2^{5/2}$.

The flow is assumed to be independent of the coordinate s. Thus, the problem is treated in the plane (r,θ), in the domain $0 \leqslant r \leqslant 1$, $-\pi/2 \leqslant \theta \leqslant 3\pi/2$. Following the commonly used notation[12,18–20] we call the velocity component w "axial velocity," and the flow in the (r,θ) plane "transverse flow."

The no-slip boundary conditions are imposed on the pipe wall

$$r=1, \quad -\pi/2 \leqslant \theta \leqslant 3\pi/2: \quad \mathbf{v} = 0, \tag{5}$$

also

$$r=0: \quad |\mathbf{v}| < \infty, \tag{6}$$

and continuity of the velocities and tangent stresses is required on the liquid–liquid interface

$$\theta = \pm\pi/2, \quad 0 \leqslant r \leqslant 1: \quad u_1 = u_2, \quad v_1 = v_2 = 0, \quad w_1 = w_2, \tag{7}$$

$$\frac{\partial u_1}{\partial \theta} = \mu_{21}\frac{\partial u_2}{\partial \theta}, \quad \frac{\partial w_1}{\partial \theta} = \mu_{21}\frac{\partial w_2}{\partial \theta}. \tag{8}$$

With the steady-state flow calculated, the mass transfer problem is considered. Here we assume that the time needed to reach the steady state of the flow is much shorter than the characteristic diffusion time, so that the mass transfer during the transient stage is negligible. The mass transfer equations are

$$\frac{\partial c_1}{\partial t} + (\mathbf{v}_1 \cdot \nabla)c_1 = \frac{1}{\text{Pe}}\Delta c_1, \tag{9}$$

$$\frac{\partial c_2}{\partial t} + (\mathbf{v}_2 \cdot \nabla)c_2 = \frac{D_{21}}{\text{Pe}}\Delta c_2, \tag{10}$$

where c_k, $k=1,2$, are the concentrations of a passive scalar in the liquid layers 1 and 2, $D_{21} = D_2/D_1 = O(1)$ is the ratio of the diffusion coefficients, $\text{Pe} = R\,\text{Sc} = (a/D_1)\sqrt{G_1 a/\rho_1}$ the Peclet number and $\text{Sc} = \mu_1/D_1\rho_1$ the Schmidt number. The excess dimensionless concentration of solute is $c = (c - c_{\min})/(c_{\max} - c_{\min})$, where $c_{\max}$ and $c_{\min}$ are the maximal and minimal concentration values at $t=0$. Initially, liquid 1 is assumed to contain a uniformly distributed admixture at a concentration $c_{\max}$, $c=1$, which begins to diffuse into the

admixture-free liquid 2 ($c_{\min} = 0$, $c = 0$). The torus is assumed to be impermeable for the admixture, while the concentrations and mass fluxes are continuous at the interface. Thus the boundary and initial conditions for the mass transfer problem read

$$r=0: \quad c_1 < \infty, \quad c_2 < \infty, \tag{11}$$

$$r=1, \quad -\pi/2 \leqslant \theta \leqslant 3\pi/2: \quad \frac{\partial c}{\partial r} = 0, \tag{12}$$

$$\theta = \pm\pi/2, \quad 0 \leqslant r \leqslant 1: \quad c_1 = c_2, \quad \frac{\partial c_1}{\partial \theta} = D_{21}\frac{\partial c_2}{\partial \theta}, \tag{13}$$

$$t=0: \quad c_1 = 1, \quad c_2 = 0. \tag{14}$$

For characterization of the mass transfer we introduce the local Sherwood number

$$\text{Sh}(x) = \frac{1}{r}\left.\frac{\partial c_2}{\partial \theta}\right|_{\theta = \pm\pi/2}, \quad x = -r\sin(\theta), \tag{15}$$

and the mass fraction that has diffused into the liquid layer 2

$$m_f = \frac{2}{\pi}\int_{\pi/2}^{3\pi/2}\int_0^1 rc_2(r,\theta)\,dr\,d\theta, \tag{16}$$

where $\pi/2$ is the area of half the dimensionless pipe cross section of unit radius. The local Sherwood number (15) is unobtainable near $r=0$ and should be calculated separately for $x<0$ and $x>0$ or, respectively, $\theta = +\pi/2$ and $\theta = -\pi/2$. It is emphasized that in our discussion of the mass transfer we use the flow pattern and x axis corresponding to cross section A of Fig. 1.

The problems (1)–(8) and (9)–(14) were solved numerically. The finite volume method was used with the SIMPLE velocity-pressure decoupling algorithm and a semi-implicit three-level time integration scheme. It was used for swirling flows in a cylindrical container[21] and for study of mass-transfer enhancement due to Taylor[3] and natural convection vortices. The code was validated additionally for single-fluid flow against the analytical solution for small R, ε, Re, and D (see Appendix B) and against the results of Refs. 13, 22, and 23 for relatively large Dean numbers. The steady-state fluid flow could be calculated with a dimensionless time step $\tau = 0.1$ for $\text{D} \leqslant 200$, and with $\tau = 0.01$ for $200 \leqslant \text{D} \leqslant 6000$ (usually, several thousands of time steps are needed to reach a converged solution at large D).

To ensure numerical stability of the mass transfer calculations at the large Peclet numbers characteristic of proteins ($\text{Pe} \sim O(10^5)$), the calculations were performed with a smaller time step $\tau = 10^{-3}$. The reported flow and mass-transfer calculations were done on the same uniform staggered grid. Jumps of the physical properties over the liquid–liquid interface were smoothed as in Ref. 3. To ensure mesh- and time-step independence of the results, the calculations for the largest value of the Peclet number ($\text{Pe} = 10^5$) were repeated on 100×200 and 150×300 grids in the r and θ directions, respectively, with time steps $\tau = 10^{-3}$ and 10^{-4}.
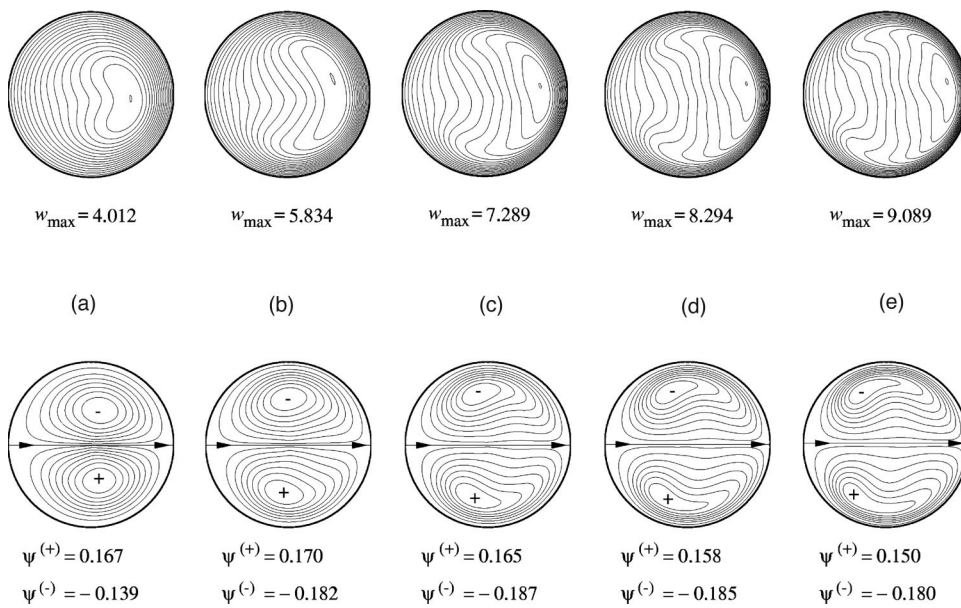
FIG. 2. Isolines of the axial velocity w (upper frames) and streamlines of the transverse flow (lower frames) for cocurrent flow $G_{21}=1$. The left-hand side of each frame corresponds to the inner part of the toroidal boundary, the right-hand side to the outer part. The cross-section B of Fig. 1 is shown. (a) $R=20$ (D=179); (b) $R=40$ (D=716); (c) $R=60$ (D=1610); (d) $R=80$ (D=2862); (e) $R=100$ (D=4472). In all cases $\varepsilon=0.1$, $\mu_{12}=0.96$.

No significant changes were found. Most of the mass-transfer results reported in the following refer to the 100×200 grid and $\tau=10^{-3}$.

Following Ref. 24 we define the characteristic turnover, averaging, and diffusion time as $T_e=(\rho_1 a/G_1)^{1/2}$, $T_a=T_d \mathrm{Pe}^{-2/3}$, $T_d=a^2/D_1$, respectively. Using, as before, the time scale $(\rho_1 a/G_1)^{1/2}$, we obtain the following dimensionless values: $T_e=1$, $T_a=\mathrm{Pe}^{1/3}$, $T_d=\mathrm{Pe}$. In the calculations reported in the following $10^3 \leqslant \mathrm{Pe} \leqslant 10^5$. The range of integration in time for the mass-transfer problem was 200 for $\mathrm{Pe}=10^3$, 1000 for $\mathrm{Pe}=10^4$, and 10 000 for $\mathrm{Pe}=10^5$, i.e., the integration time was always longer than the averaging time and shorter than the diffusion time.

III. RESULTS AND DISCUSSION

In the calculations the parameter R was varied from 1 to 100 or 120 and the Peclet number Pe from 10^3 to 10^5. Thus,

the maximal Schmidt number $\mathrm{Sc}=\mathrm{Pe}/R$ was 10^3 for $R=100$ and even larger for smaller R. The dimensionless curvature of the tube was typically taken as $\varepsilon=0.1$. The variation of R in the range $1 \leqslant R \leqslant 120$ corresponds to that of the Dean number $0.45 \leqslant \mathrm{D} \leqslant 6440$. The other governing parameters were fixed. We considered the cases of cocurrent and countercurrent axial flow in the two layers, corresponding to $G_{21}=1$ and -1, respectively. In most of the calculations the fixed property ratios of the liquids were chosen as $\rho_{21}=1.4$, $\mu_{21}=0.96$, and $D_{21}=1.1$, and the values of the density and viscosity ratios were taken from the experiment.[1] Since the physical properties of the two protein solutions should be close, the value of D_{21} was chosen close to unity.

A. Flow patterns

The calculated flow patterns in the cocurrent and countercurrent flows are plotted in Figs. 2 and 3. All the isolines
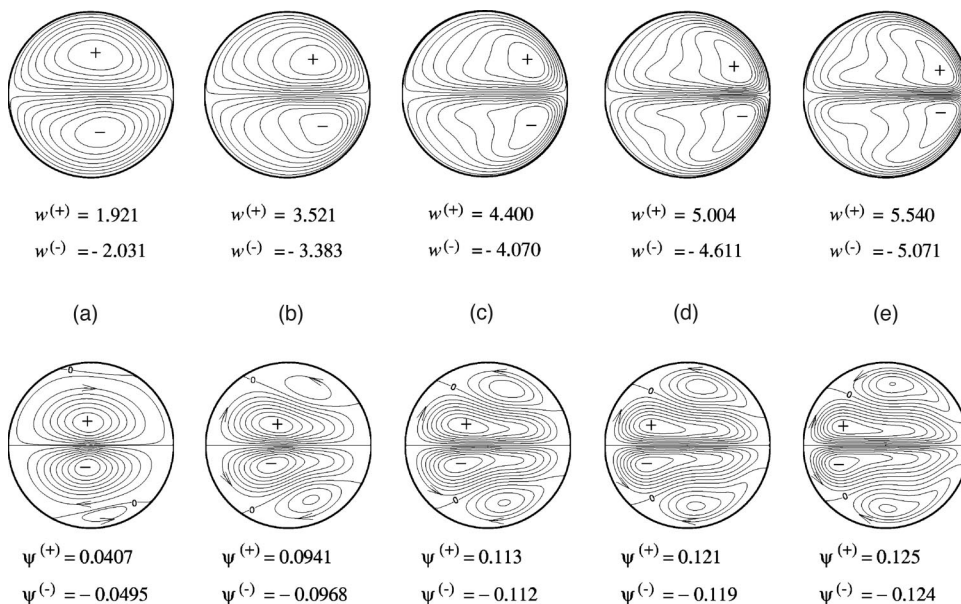

FIG. 3. Isolines of the axial velocity w (upper frames) and streamlines of the transverse flow (lower frames) for countercurrent flow $G_{21}=-1$. The left-hand side of each frame corresponds to the inner part of the toroidal boundary, the right-hand side to the outer part. The cross-section B of Fig. 1 is shown. (a) $R=20$ (D=179); (b) $R=40$ (D=716); (c) $R=60$ (D=1610); (d) $R=80$ (D=2862); (e) $R=100$ (D=4472). In all cases $\varepsilon=0.1$, $\mu_{12}=0.96$. The sections of the streamline $\psi=0$, which do not coincide with the interface, are highlighted by numeral zero.
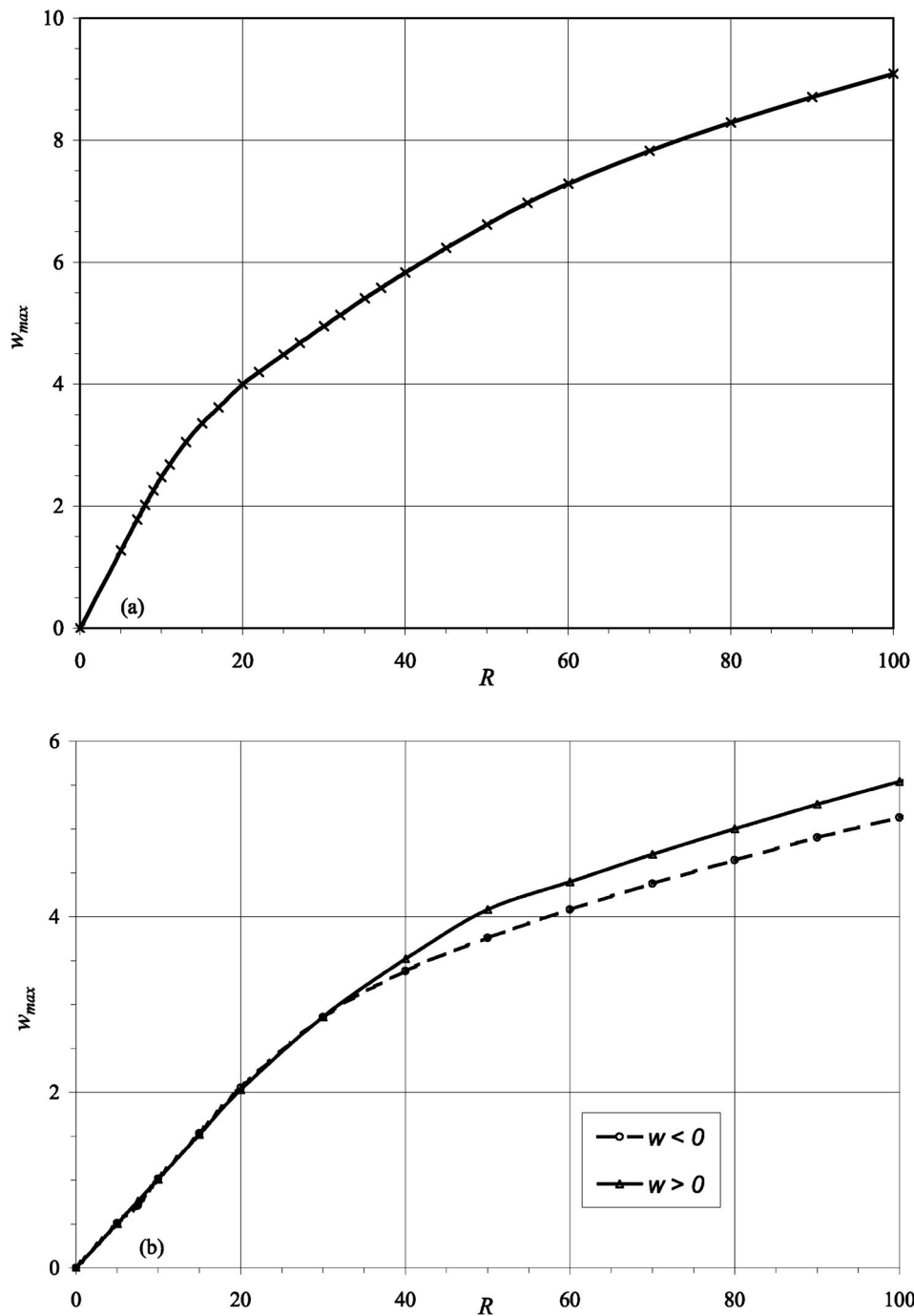
FIG. 4. Maximal values of the axial velocity vs the R number. Symbols correspond to the calculated points. The range $0 \leqslant R \leqslant 100$ corresponds to that of the Dean number $0 \leqslant D \leqslant 4472$; $\varepsilon = 0.1$. (a) Cocurrent flow, $G_{21} = 1$, (b) countercurrent flow, $G_{21} = -1$, $\mu_{12} = 0.96$.

are equally spaced, except for the streamlines in Fig. 3(a) where two additional levels are added to illustrate the appearance of additional vortices. The positive and negative contours of the stream function correspond to the clockwise and counterclockwise motion, respectively.

In the case of the cocurrent flow ($G_{21} = 1$, Fig. 2) the maximal value of the axial velocity is located close to (but not at) the center plane (note that in the single liquid case this maximum is always exactly at the center plane[3,13,18–20]). In the two-fluid case considered here the advection of the axial velocity takes place in each of the layers separately. Therefore, one can expect appearance of one maximum of the axial velocity in each layer. However, with the param-

eters used in the present calculations, development of two local maxima was not observed; it could probably happen if the density and viscosity differentials between the liquids were larger. The transverse flows consist of a pair of the Dean vortices with one vortex in each layer as in the classical Dean case of a single-liquid flow. With increase of the parameter R (i.e., of the Reynolds or the Dean numbers, Re and D), the maximum of the axial velocity is advected toward the outer part of the solid boundary, and a boundary layer of the axial velocity forms there. Also, with the increase of the parameter R (or Re and D) the ''eyes'' of the vortices are pushed backwards and outwards, as shown in Fig. 2. A similar observation was done in Ref. 7 regarding a
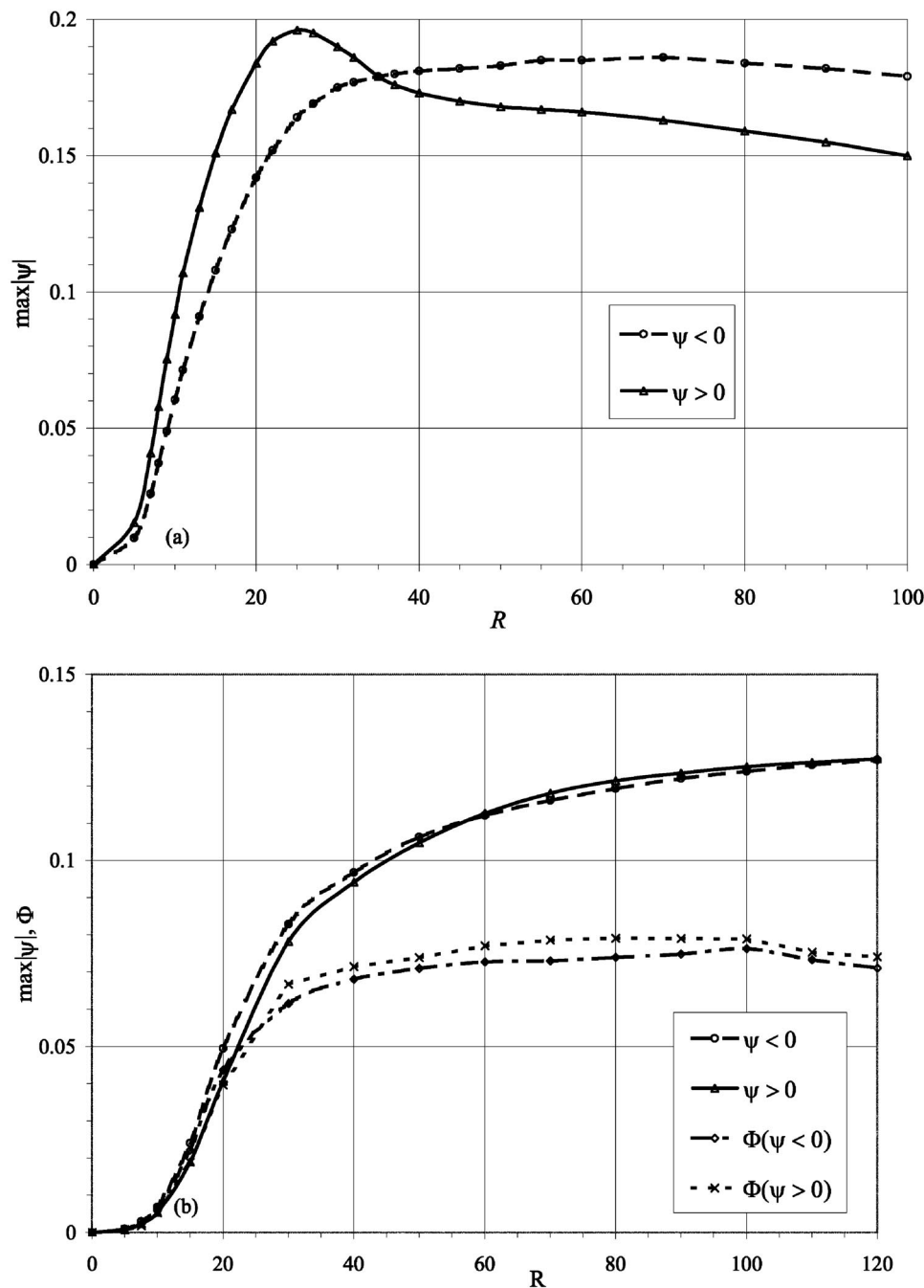
FIG. 5. Maximal values of the stream function and the quantity Φ vs the R number. The range $0 \leqslant R \leqslant 100$ corresponds to that of the Dean number $0 \leqslant D \leqslant 4472$; $\varepsilon = 0.1$. (a) Cocurrent flow, $G_{21} = 1$, (b) countercurrent flow, $G_{21} = -1$, $\mu_{12} = 0.96$.

single-fluid flow in a curved pipe, based on their numerical and experimental results. The maximum and minimum of the stream functions shift in the opposite direction—toward the inner boundary and the liquid–liquid interface. Development of the boundary layer is a common observation for the single-liquid case.[18–20] Note that due to the action of the centrifugal force, which is directed toward the outer part of the toroidal boundary and is maximal near the interface, the motion along the latter is also directed from the inner (left-hand) to the outer (right-hand) part of the solid (toroidal) boundary.

In the case of countercurrent flow ($G_{21} = -1$, Fig. 3) there are two maxima of the axial velocity, one in each layer. Near these maxima the centrifugal force drives the transverse flow toward the outer part of the boundary, so that the flow returns to the inner part along the interface. Therefore, the direction of motion along the interface is opposite to that in the cocurrent case (cf. Figs. 2 and 3). Besides this, already at rather low values of R or of the Dean number, $R \approx 10$ or $D \approx 45$, each Dean vortex of the transverse flow splits in two. It will be shown in the following that this split reduces the mixing of a passive scalar. Note also that in the case of countercurrent flow, the boundary layers develop not only near the outer part of the boundary, but also near the interface.

The dependences of the maximal absolute values of the axial velocity and the stream function on the Reynolds number are shown in Figs. 4 and 5. The axial velocity, as ex-
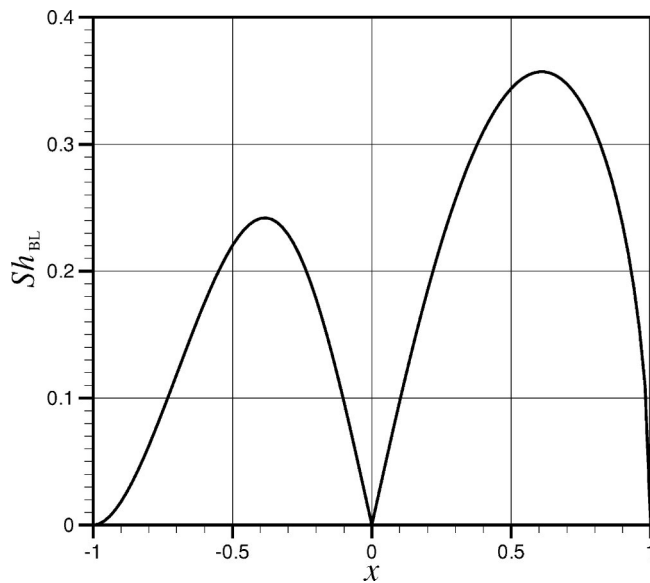
FIG. 6. Local Sherwood number calculated via the analytical boundary layer model for $R=1$ and $\varepsilon=0.01$. The Reynolds and Dean numbers are Re$=0.125$ and D$=0.141$, respectively. The value of D_{21} was chosen as $D_{21}=1$. The plot corresponds to the cross-section A of Fig. 1, $x=-1$ corresponds to the outer part of the toroidal surface, $x=1$—to the inner one. The Schmidt number was Sc$=10^5$ and thus the Peclet number Pe$=10^5$.

pected, increases monotonically (Fig. 4); the increase is linear at small values of $R<20$ ($D<179$), where viscous dissipation is significant, and slows down at larger R (or larger D).

As mentioned, in the case of cocurrent flow there is a single Dean vortex in each layer (Fig. 2). The maximal value of the stream function yields a coarse estimate of the vortex intensity, and consequently an estimate of the mixing speed of a passive scalar inside the vortex. It was unexpectedly found that in the cocurrent flow case the dependencies $\psi_{max}(R)$ are nonmonotonic and reach a maximum at a certain value of the parameter R [Fig. 5(a)]. Therefore the dependence of the mass transfer rate on the Reynolds number should also be nonmonotonic, and indeed, we shall see in the following that it also has a maximum at a certain moderate value of R (or D).

In the case of countercurrent flow the maximal absolute values of the stream function increase monotonically with the Reynolds number [Fig. 5(b)]. However, in this case there can be two vortices in each of the layers subdivided by sections of the streamline $\psi=0$, which do not coincide with the interface (Fig. 3), and part of the passive scalar should be transported through the boundary separating two *steady* vortices. Therefore, there is no direct relation between the intensity of the strongest vortices and the mixing rate of a passive scalar at the interface. To characterize the mixing rate inside a vortex (Sec. III) we introduce the following measure:

$$\Phi=\frac{2}{\pi}S_{\text{vortex}}|\psi|_{\max}, \tag{17}$$

where S_{vortex} is the dimensionless area occupied by the vortex and $\pi/2$ is the total area of the layer (the dimensionless radius of the pipe cross section is equal to 1). The area S_{vortex}

corresponds to the area occupied by the vortices bounded by the interface and the streamline $\psi=0$ marked by numeral zero in each of the layers in the lower frames in Fig. 3. The value of Φ is sensitive to both the vortex intensity $|\psi_{\max}|$ and the fraction of the layer occupied by it. Variation of the quantity Φ with R is shown in Fig. 5(b). It is seen that for $R>60$, Φ does not change strongly, and has a smooth maximum at $R\approx100$. Therefore in the countercurrent case, the mixing rate is not expected to change strongly for $60\leqslant R\leqslant120$ ($1610\leqslant D\leqslant6440$).

For aqueous solutions ($\rho_1=1$ g/cm^3 and $\mu_1=10^{-2}$ g/(cm s)) in a pipe of $a=1$ cm the pressure gradient G_1 can be estimated as 0.08 and 8 Pa/m for $R=10$ and 100, respectively. This corresponds to the respective maximal transverse velocities of approximately 0.11 and 2.8 cm/s for the cocurrent, and to 0.045 and 1.9 cm/s for the countercurrent flow. The smaller maximal transverse velocity in the latter case reflects the splitting of the vortices in each fluid layer in the former. For comparison, the velocity of the secondary meridional flow in a two-layer Taylor–Couette apparatus[3] was found to be of the order of 0.6 cm/s under realistic conditions, and the velocity of a two-layer natural convection flow was estimated as 0.17 cm/s. The results show that the Dean vortices in two-layer systems are stronger than the corresponding Taylor–Couette or natural-convection counterparts. Thus novel bioseparators based on the Dean vortices can be expected to be more effective than those based on the Taylor–Couette apparatus. This fact is a consequence of the nature of the Dean and Taylor–Couette vortices: the former appear at any flow rate as an intrinsic part of the basic flow, and the latter—as a result of bifurcation of the secondary flow from the basic one beyond a certain threshold. Thus the Dean vortices take up a significantly larger amount of the flow energy than the Taylor–Couette ones, and are accordingly stronger than the latter.

B. Mass transfer

A general analytical solution for quasistationary mass transfer through a liquid–liquid interface between a pair of counterrotating vortices is given in Ref. 4 for large Peclet numbers. In the case of Pe$\gg1$ the mass transfer takes place in a thin boundary layer adjoining the interface, whereas far from this layer the concentration can be assumed to be constant. The local Sherwood number, corresponding to the quasistationary concentration distribution, can then be expressed as a function of the interfacial velocity. In the present case the only analytical flow field available is the one corresponding to a single-liquid case at small values of the Dean number (cf. (B5)–(B9) in Appendix B). It is appliable to the two-layer cocurrent ($G_{21}=1$) case only at $\rho_{21}=\mu_{21}=1$ and $D\rightarrow0$, for which we undertake to derive an analytical solution for the mass transfer rate. Then, employing the general solution[4] for the concentration field and Eq. (C19) (see Appendix C), we arrive in the present case at the following result:
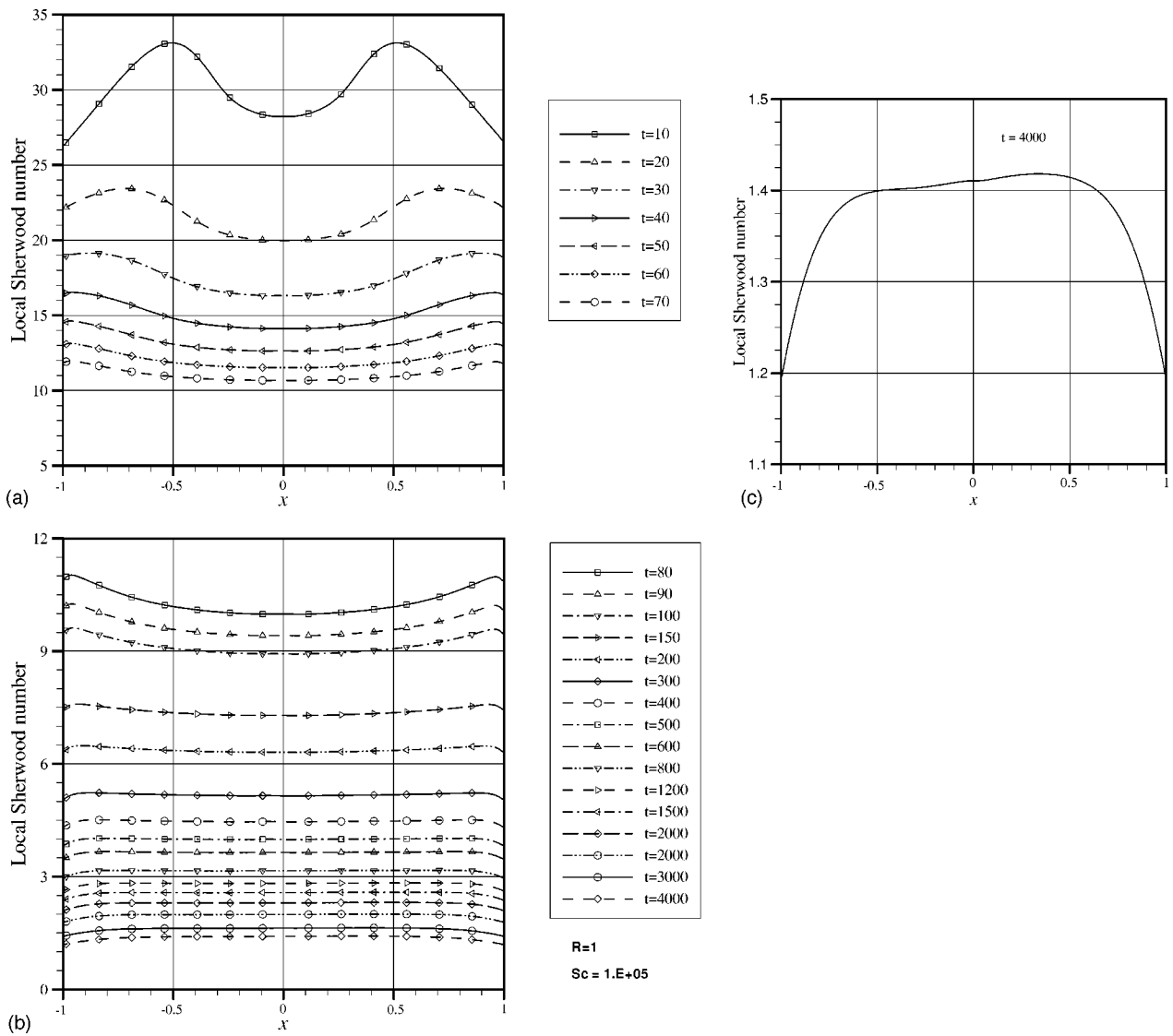
FIG. 7. The instantaneous local Sherwood number calculated for $R=1$, $\varepsilon=0.01$, $G_{21}=1$, $D_{21}=1$, and $Pe=10^5$. The Reynolds and Dean numbers are Re $=0.125$ and D$=0.141$, respectively. The x axis represents the liquid–liquid interface, $x=-1$ corresponding to the outer part of the toroidal pipe, and $x=1$—to the inner part. The cross-section A of Fig. 1 is shown. (a) $10 \leqslant t \leqslant 80$, (b) $80 \leqslant t \leqslant 4000$, (c) $t=4000$.

$$\mathrm{Sh_{BL}}(x) = \frac{1}{48\sqrt{\pi}} \mathrm{D}\ \mathrm{Sc}^{1/2} \frac{D_1/D_2}{1+\sqrt{D_1/D_2}} f(x), \quad -1 \leqslant x \leqslant 1,$$
(18)

where $\mathrm{Sc}=\mu_1/(\rho_1 D_1)$. The function $f(x)$ is given by

$$f(x) = \frac{|x|(1-x^2/4)(1-x^2)^2}{[22/315 - x^3/3 + 9x^5/20 - 3x^7/14 + x^9/36]^{1/2}}.$$
(19)

It is readily seen that $\mathrm{Sh_{BL}}(\pm 1)=0$.

Figure 6 shows the local Sherwood number $\mathrm{Sh_{BL}}$ calculated as per Eqs. (18) and (19) for $R=1$ and $\varepsilon=0.01$. The profile of $\mathrm{Sh_{BL}}(x)$ is characterized by a zero value in the middle of the interface and two local maxima, with the larger maximum corresponding to the inner part of the flow along the interface. Cross-section A of Fig. 1 corresponds to the results in Fig. 6.

The instantaneous local Sherwood numbers obtained via time-dependent numerical modeling for the above-mentioned case ($R=1$, $\varepsilon=0.01$, $G_{21}=1$, $\eta_{21}=\rho_{21}=D_{21}=1$) using the

model (9)–(14)—are shown in Figs. 7 and 8 for $Pe=10^5$ and 10^6, respectively. Cross-section A of Fig. 1 corresponds to these results as well.

At $Pe=10^5$ and relatively short integration times (Fig. 7(a)) the local Sherwood number is distributed almost symmetrically about the central point $x=0$ and has two almost equal maxima located to the right and left of the central point. With increase of the integration time, the mass transfer in the central part of the interface intensifies, so that these two maxima disappear (Fig. 7(b)). At long integration times ($t>500$), the local Sherwood number slowly decreases with time and its profile approaches a certain asymptotic shape, illustrated in Fig. 7(c). At a long integration time the profile is characterized by slow variation in the central part of the boundary and a steep decrease near the boundaries.

For $Pe=10^6$ and short integration times, $t<500$, the distribution of the local Sherwood number is likewise characterized by two almost equal and symmetric maxima (Figs. 8(a) and 8(b)). With increase of the integration time, these
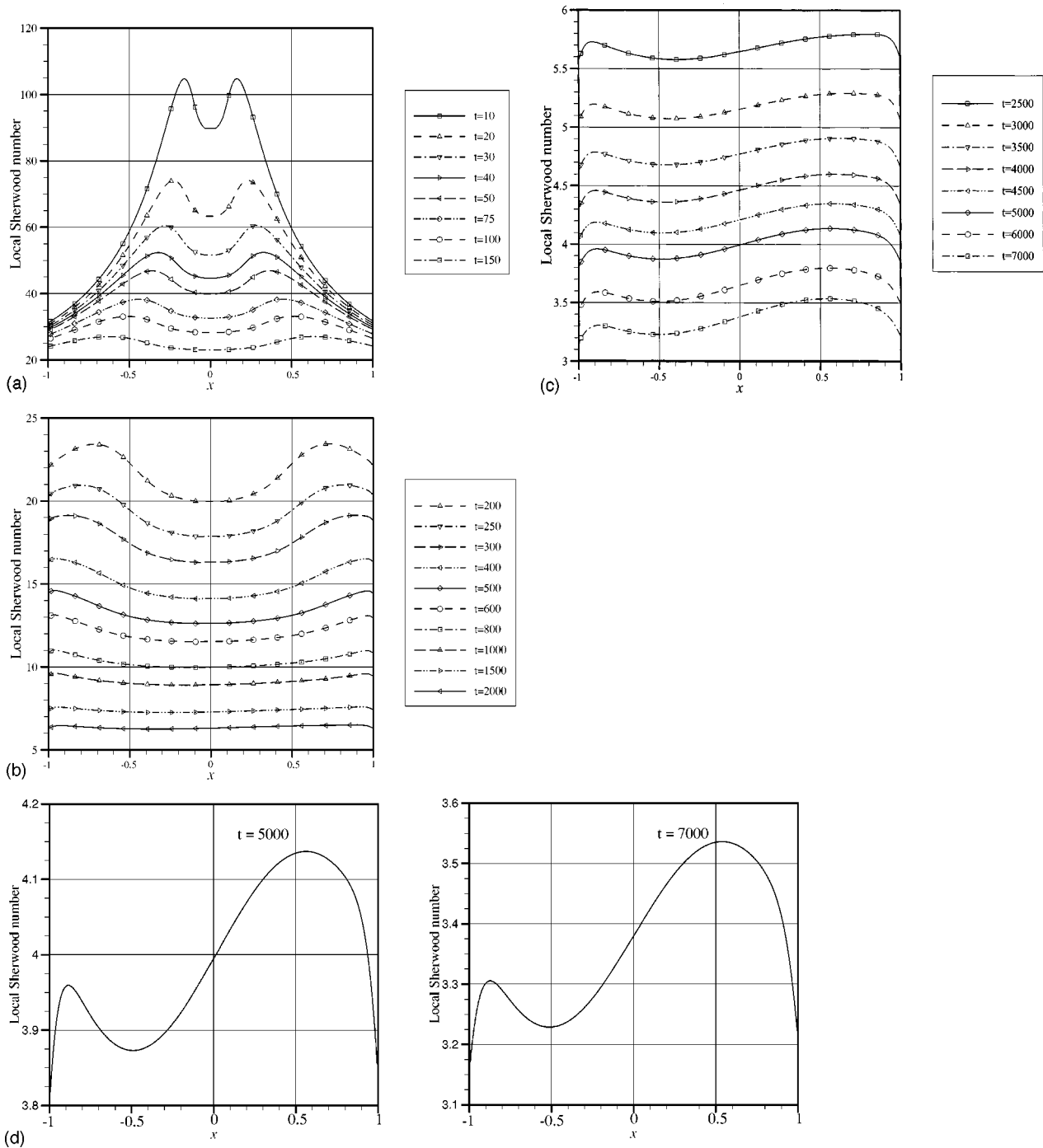
FIG. 8. The instantaneous local Sherwood number calculated for $R=1$, $\varepsilon=0.01$, $G_{21}=1$, $D_{21}=1$, and $Pe=10^6$. The Reynolds and Dean numbers are $Re=0.125$ and $D=0.141$, respectively. The x axis represents the liquid–liquid interface, $x=-1$ corresponding to the outer part of the toroidal pipe, and $x=1$—to the inner part. The cross-section A of Fig. 1 is shown. (a) $10 \leq t \leq 150$, (b) $200 \leq t \leq 2000$, (c) $2500 \leq t \leq 5000$, (d) $t=5000$ and 7000.

maxima are shifted from the central part of the interface toward the boundaries. At larger times, $t > 2000$, the profile likewise acquires an asymptotic shape (Fig. 8(c)), qualitatively different from that for $Pe=10^5$. The profiles at $t=5000$ and 7000 are zoomed in Fig. 8(d) and are seen to have two non-symmetric and nonequal maxima, the larger one near the inner part of the torus boundary ($x=1$) and the smaller one—near the outer part ($x=-1$). This agrees qualitatively with the analytical result (18) and (19) as per Fig. 6. In agreement with the analytical boundary layer

model, the profiles have a rather steep minimum between the two maxima, but unlike the former the minimum is located near $x=-0.5$ instead of the analytically predicted $x=0$. The magnitudes of the local Sherwood number at the maxima in Fig. 8(d) are also significantly larger than those in Fig. 6. This shows that steady-state mass transfer has not yet been achieved in Fig. 8(d). Closer agreement with the analytical model may perhaps be obtained for larger Peclet numbers, e.g., $Pe=10^7$ or 10^8. However, in this case much finer grids
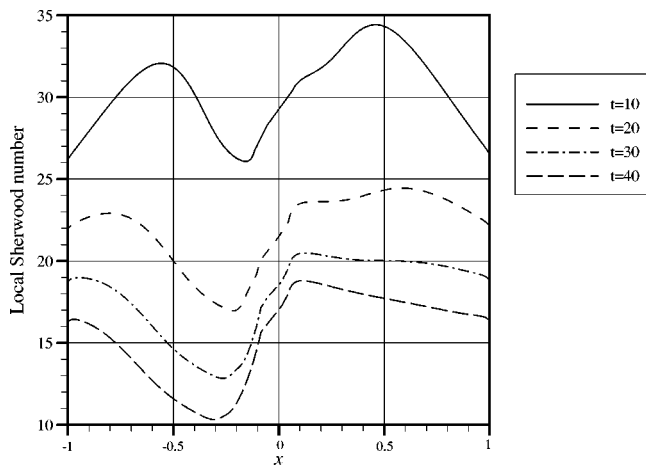
Phys. Fluids, Vol. 15, No. 2, February 2003

Dean vortices-induced enhancement   339

FIG. 9. The instantaneous local Sherwood number calculated for $R=10$, $\varepsilon=0.01$, $G_{21}=1$, $D_{21}=1$, and $Pe=10^5$. The Reynolds and Dean numbers are Re=12.5 and D=14.1, respectively. The x axis represents the liquid–liquid interface, $x=-1$ corresponding to the outer part of the toroidal pipe, and $x=1$—to the inner part. The cross-section A of Fig. 1 is shown.

and calculation over much longer times will be required, which makes the process unaffordable.

Profiles qualitatively similar to the analytical one can also be observed at larger R numbers at very short integra-

tion times. This is illustrated in Fig. 9. The calculations were performed for $R=10$, $\varepsilon=0.01$, $G_{21}=1$, and $\eta_{21}=\rho_{21}=D_{21}=1$. The profiles have two maxima with the larger maximum near the inner part of the torus boundary, as predicted by the analytical model, and the minimum closer to the center of the interface $x=0$ (cf. Fig. 8(d)) and shifting toward $x=-0.5$ as time increases. This deviation from the analytical prediction can be explained by mixing of the admixture inside the bulk of the Dean vortices, which affects the boundary conditions for the interfacial mass transfer already at a very early stage of the process.

The instantaneous concentration fields at large Reynolds and Peclet numbers, Re=100 and $Pe=10^5$, are shown in Figs. 10 and 11. It is seen that the concentration isolines reproduce the streamlines of the transverse flow in the bulk of both liquids (cf. Figs. 2 and 3). This means that at the large Peclet number, the mass transfer is almost completely dominated by the convective transport due to the transverse flow. However, diffusion represents the only mechanism of mass transfer through the interface. As was shown in Ref. 3, enhancement of the mass transfer is due to the steeper concentration gradients at the interface created by the enhanced convective transport of the admixture. This leads to a higher mass flux even though the diffusion coefficients continue to be low. The corresponding distributions of the local Sher-
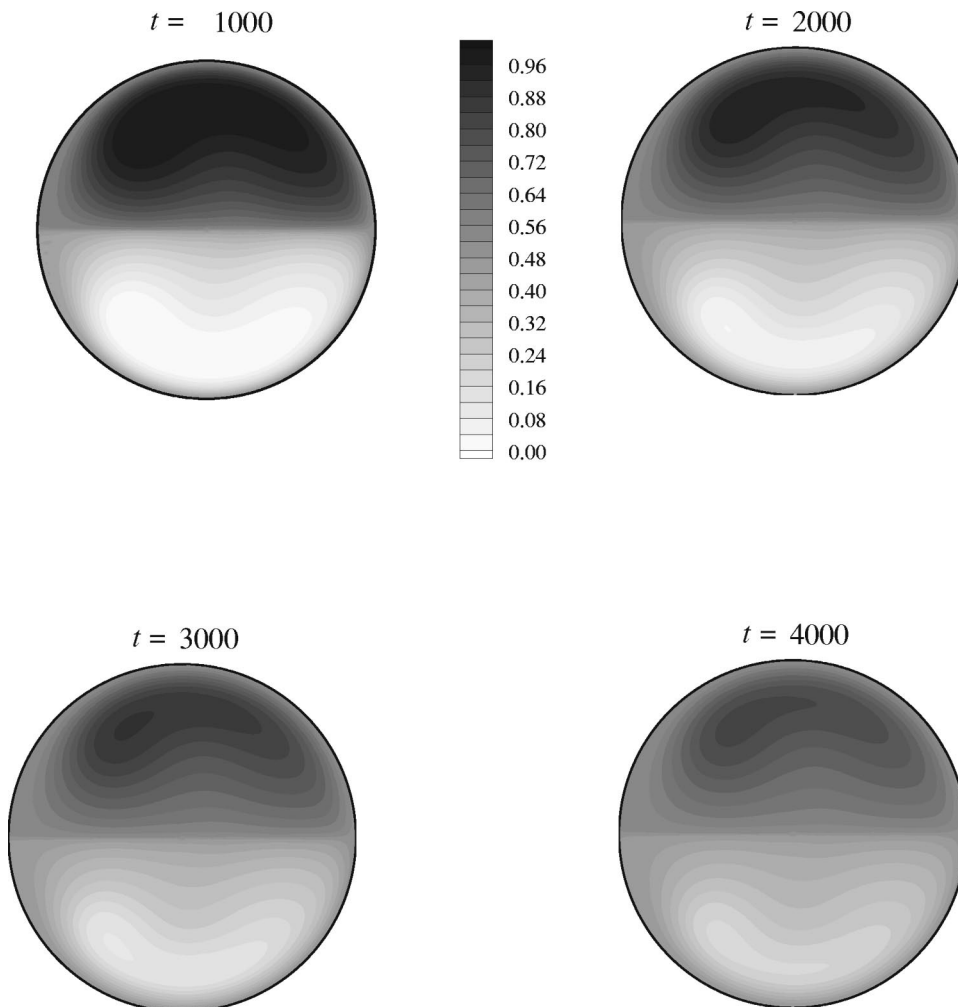

FIG. 10. The instantaneous concentration contours at different time moments. The case of cocurrent flow, $G_{21}=1$, $\varepsilon=0.1$, $R=100$, and $Pe=10^5$ (D=4472). 25 concentration contours are equally distributed between $c=0$ and $c=1$. The cross-section B of Fig. 1 is shown.
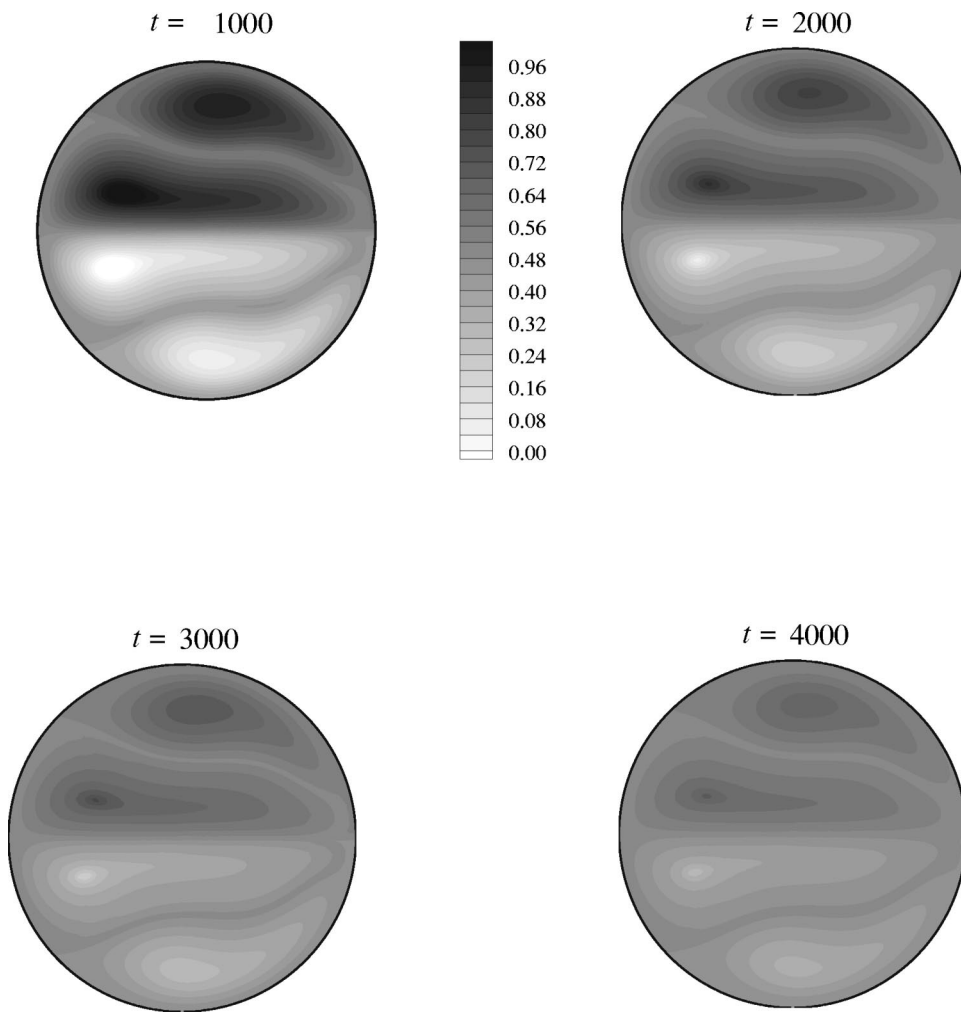
FIG. 11. The instantaneous concentration contours at different time moments. The case of countercurrent flow, $G_{21} = -1$, $\varepsilon = 0.1$, $R = 100$, and Pe$= 10^5$ (D$=4472$). 25 concentration contours are equally distributed between $c = 0$ and $c = 1$. The cross-section B of Fig. 1 is shown.
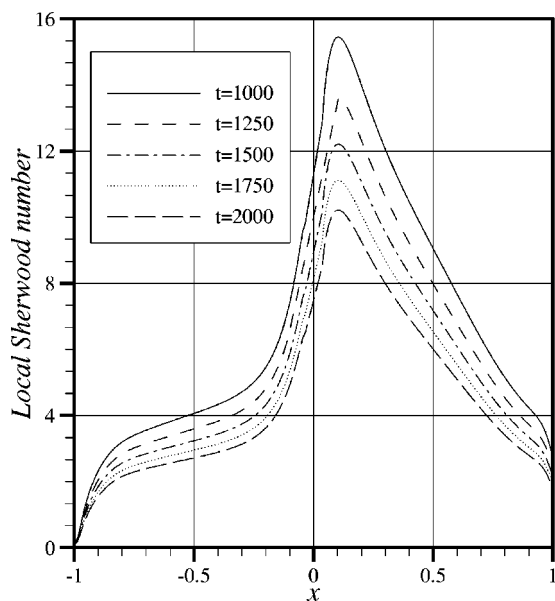

FIG. 12. The instantaneous local Sherwood number at different time moments. The case of cocurrent flow, $G_{21} = 1$, $\varepsilon = 0.1$, $R = 100$ (D$=4472$), and Pe$= 10^5$. The cross-section A of Fig. 1 is shown.
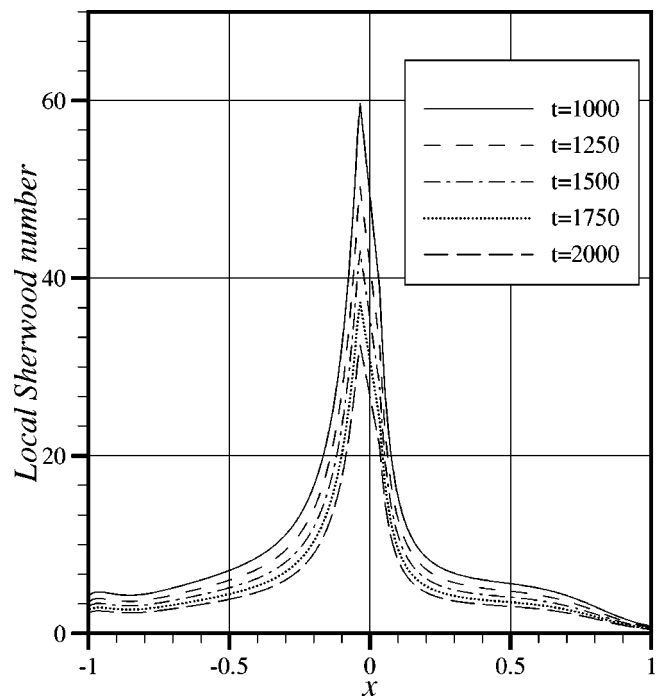
FIG. 13. The instantaneous local Sherwood number at different time moments. The case of countercurrent flow, $G_{21} = -1$, $\varepsilon = 0.1$, $R = 100$ (D $=4472$), and Pe$= 10^5$. The cross-section A of Fig. 1 is shown.
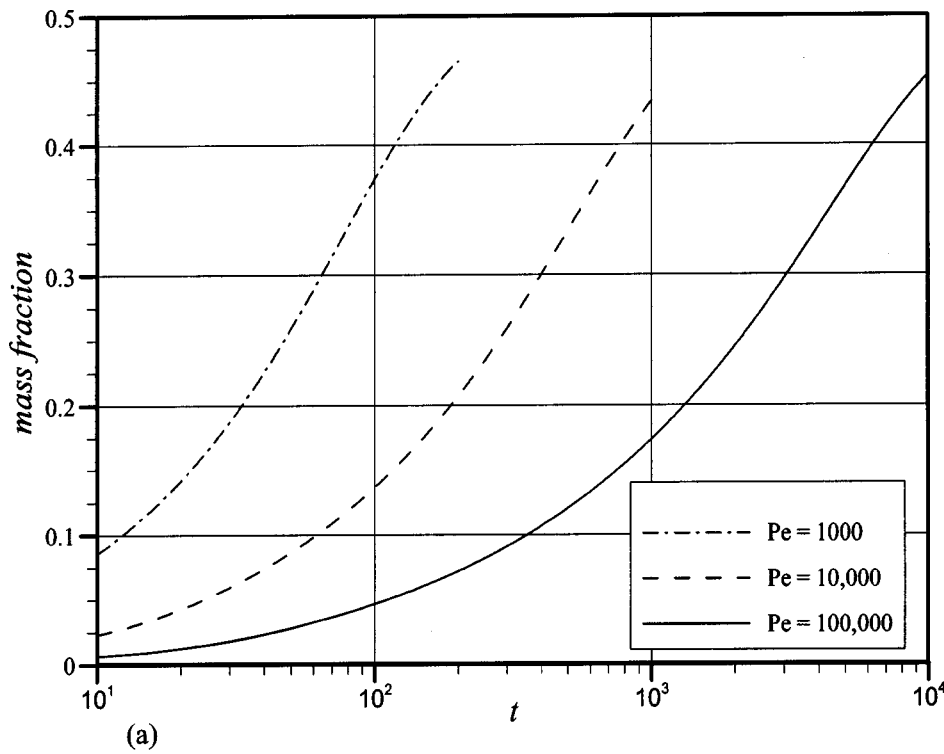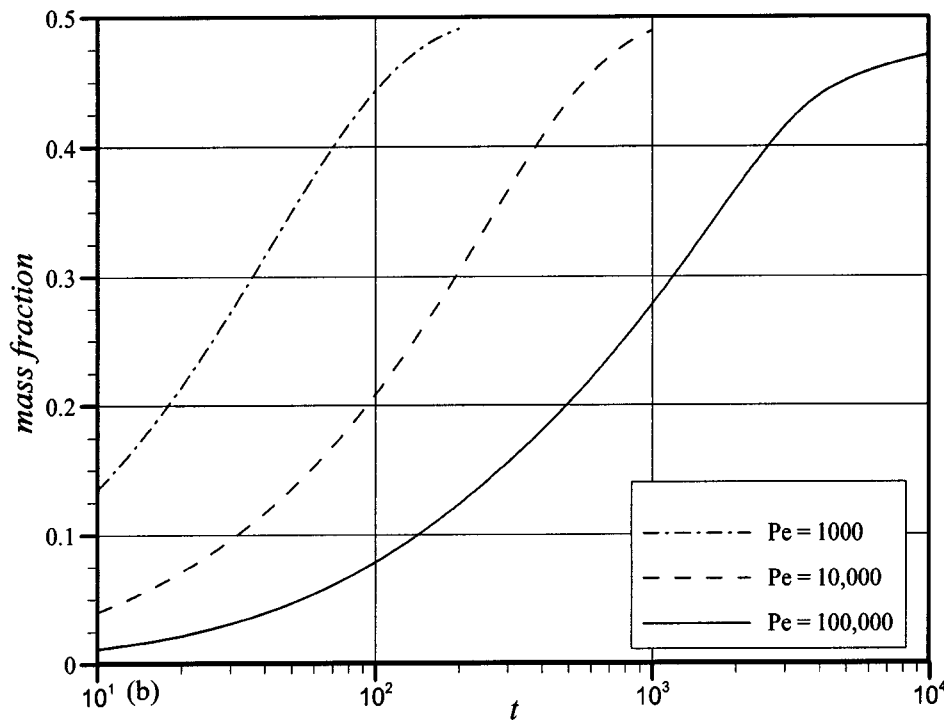
FIG. 14. Time histories of the mass fraction m_f in layer 2. $R=100$ (D $=4472$). (a) Cocurrent flow, $G_{21}=1$, (b) countercurrent flow, $G_{21}=-1$, $\mu_{12}=0.96$.

wood number over the interface are shown in Figs. 12 and 13. In the case of cocurrent flow (Fig. 2) the local Sherwood number increases starting from the inner part of the flow region, $x=-1$ (where the streamlines in the two layers become closer near the interface) and then decays toward the outer part, $x=1$. In the case of countercurrent flow (Fig. 3) the direction of the interfacial flow is opposite, and the local Sherwood number increases from the outer boundary and

then decreases as the inner one is approached. In both cases the Sherwood number is larger in the areas where the liquid motion in the vortices is directed toward the interface. The rapid growth of Sh(x) near $x=0$ should not be overestimated, since a significant numerical error may be involved there (see Eq. (15)), but still the distributions corresponding to higher values of the Dean number (or the higher values of R) are radically different from those for D→0. Indeed, com-
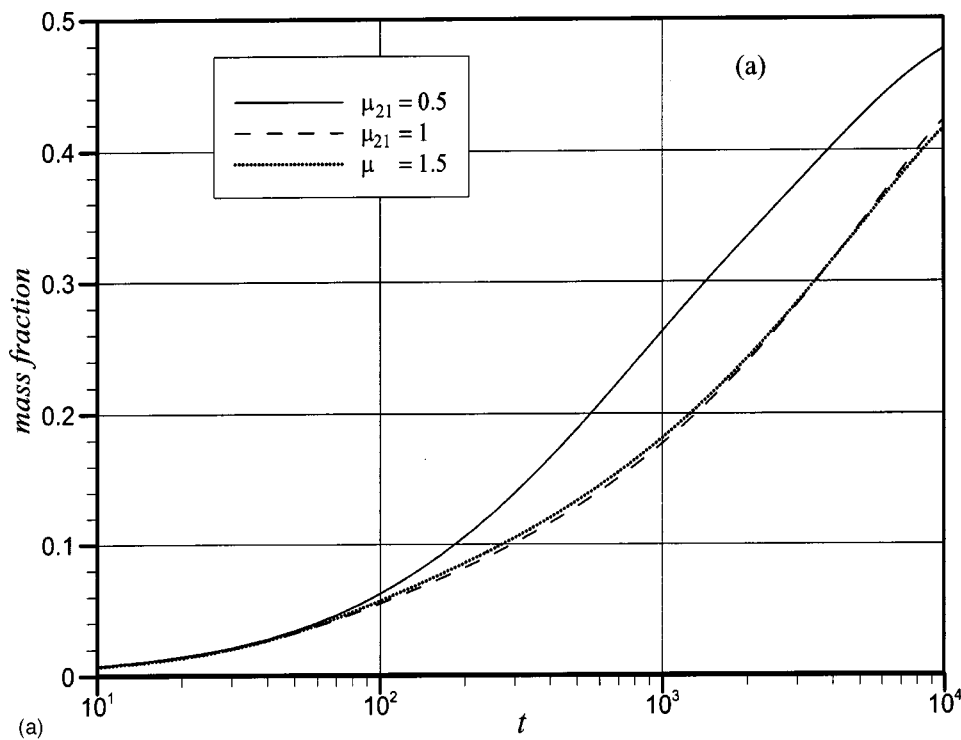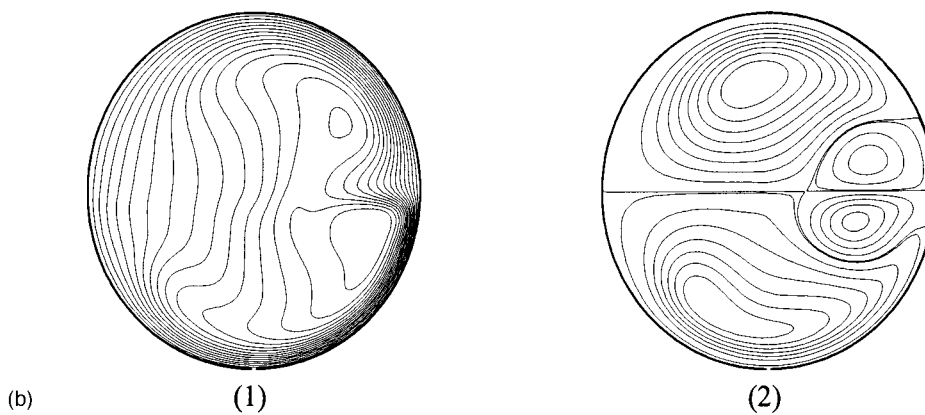
FIG. 15. (a) Time histories of the mass fraction m_f in layer 2 for different viscosity ratios μ_{12}. $R=50$ (D=1118), Pe=10^5, $\varepsilon=0.1$. Cocurrent flow, $G_{21}=1$. (b) Isolines of the axial velocity (1) and streamlines of the transverse flow (2). $R=50$ (D=1118), Pe=10^5, $\varepsilon=0.1$. Cocurrent flow, $G_{21}=1$, $\mu_{12}=0.5$.

parison of Figs. 6, 7, and 12 shows that the minimum of Sh at the pipe center, characteristic of D→0, disappears for higher values of D.

Time histories of the mass fraction m_f (Eq. (16)) in layer 2 are shown in Fig. 14 for $R=100$ (D≈4500) and the Peclet number varying from 10^3 to 10^5. With increase of the Peclet number, the mass transfer slows down, since the limiting purely diffusional transport through the interface becomes weaker. The dimensionless time necessary to reach about 90% of complete equilibration of the admixture concentration in both layers can be estimated as Pe/10.

The effect of the viscosity ratio μ_{12} is illustrated in Figs. 15 and 16 for the cocurrent and countercurrent flows, respectively. It is seen (Fig. 15(a)) that for the cocurrent flow mass transfer increases significantly for $\mu_{12}=0.5$. This results from the fact that a single-vortex system in each fluid layer characteristic of the values $\mu_{12}=0.96–1.5$ (cf. Fig. 2) is replaced in the case of $\mu_{12}=0.5$ by a double-vortex system in
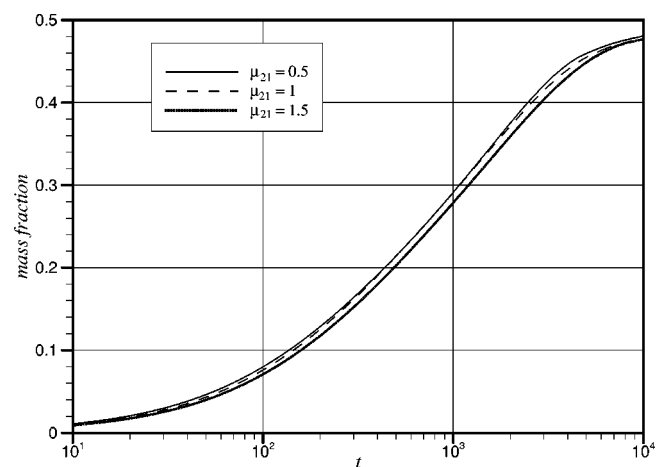

FIG. 16. Time histories of the mass fraction m_f in layer 2 for different viscosity ratios μ_{12}. $R=50$ (D=1118), Pe=10^5, $\varepsilon=0.1$. Countercurrent flow, $G_{21}=-1$.
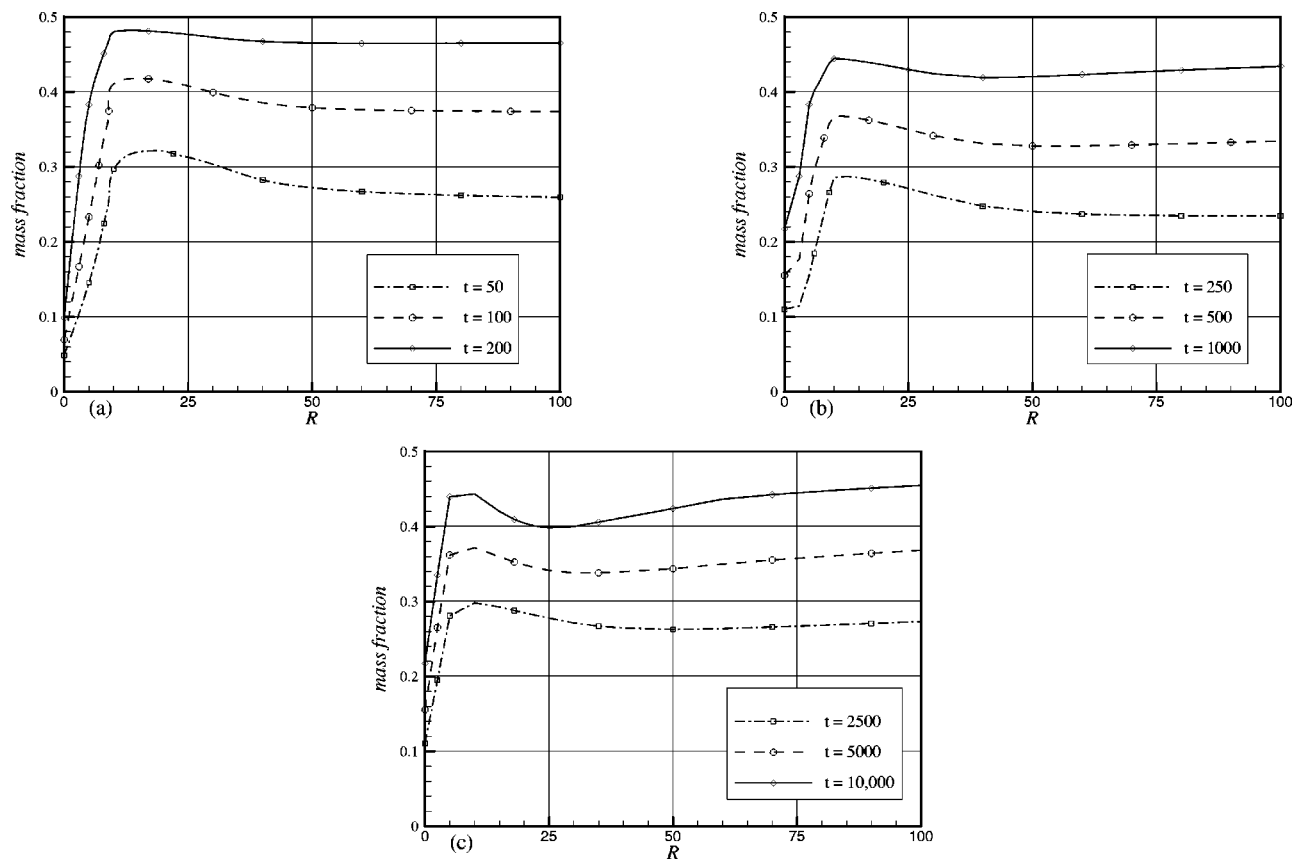
FIG. 17. Volume fraction m_f in layer 2 vs the parameter R (or the Dean number at three different times). Cocurrent flow, $0 \leqslant R \leqslant 100$, $0 \leqslant D \leqslant 4472$, $G_{21} = 1$, $\mu_{12} = 0.96$. (a) Pe$= 10^3$, (b) Pe$= 10^4$, (c) Pe$= 10^5$.

each fluid layer (Fig. 15(b)). On the other hand, the effect of viscosity ratio μ_{12} on the mass transfer rate in countercurrent flows is relatively small (Fig. 16).

To illustrate how the Dean vortices in two-layer systems enhance the mass transfer, the mass fraction m_f at several fixed time moments is plotted in Figs. 17 and 18 versus the parameter R (or the Dean number) for several Peclet numbers. It is seen that increase of R from 0 to approximately 10 or 15 (increase of D from 0 to about 45 or 100) leads to steep increase of the mass transfer rates in both the cocurrent and countercurrent flows. Further increase of R (or of the Dean number) does not yield any significant increase of the mass transfer and sometimes even a slight reduction (Fig. 17). Note that the trend of variation of the mass transfer rate with R (or with the Dean number) corresponds to the trend of intensity of the vortical motion illustrated in Fig. 5. In the case of cocurrent flow (Figs. 2 and 5(a)) the stream function reaches its largest value at $R \approx 25$ (D≈ 280) and then virtually saturates versus R (or D). Figure 17 shows that the mass transfer affected by this flow, steeply intensifies up to $R \approx 15$ (D≈ 100) and then likewise practically saturates. The position of the maximum of m_f in Figs. 17(a)–17(c) is almost independent of the Peclet number. Thus, the dependence of the mass transfer rate on the parameter R (or on the Dean number) correlates with the corresponding dependence of the vortex intensity (cf. Figs. 5(a) and 17). In the case of countercurrent flow (Figs. 3 and 5(b)) the maximum of the stream function of the transverse flow, as well as the quantity

Φ, steeply increase up to $R \approx 40$ (D≈ 715), and at larger values of R the quantity Φ almost saturates. The increase of the mass transfer rate in this case (cf. Fig. 18) corresponds to the range $R < 50$ (D< 1118), which also correlates with the estimated intensity of the vortices adjoining to the liquid–liquid interface. The steep growth of the mass fraction (and, therefore, of the mass transfer rate) in the countercurrent case of Fig. 18 corresponds to Re< 25 (D< 280) at Pe$= 10^3$, to $R < 20$ (D< 180) at Pe$= 10^4$, and to $R \approx 15$ (D< 100) at Pe$= 10^5$. This means that there exists an optimal value of the parameter R (an optimal axial flow rate), which yields the most effective mass transfer through the liquid–liquid interface. This optimal value depends on the Peclet number, on the pipe curvature, and on the mode of axial flow (cocurrent or countercurrent). In any case, it is not very large and can be roughly estimated as $R \approx 20$, which corresponds to Re≈ 50 or D≈ 180 for $\varepsilon = 0.1$. From the practical point of view this means that optimal mass transfer enhancement is reached at a moderate pressure drop, and there is no need to increase the axial flow rate beyond a certain point. This conclusion is valid for both the cocurrent and countercurrent cases, which do not differ too much.

It should be noted that we did not find any well-defined power scaling in the dependence of the intensity of the transverse flow on the parameter R (or on the Reynolds and Dean numbers; cf. Fig. 5). As a result, there is no power-law scaling of the mass transfer rate versus the Peclet number either. Finally, it is emphasized that the effect of variation of
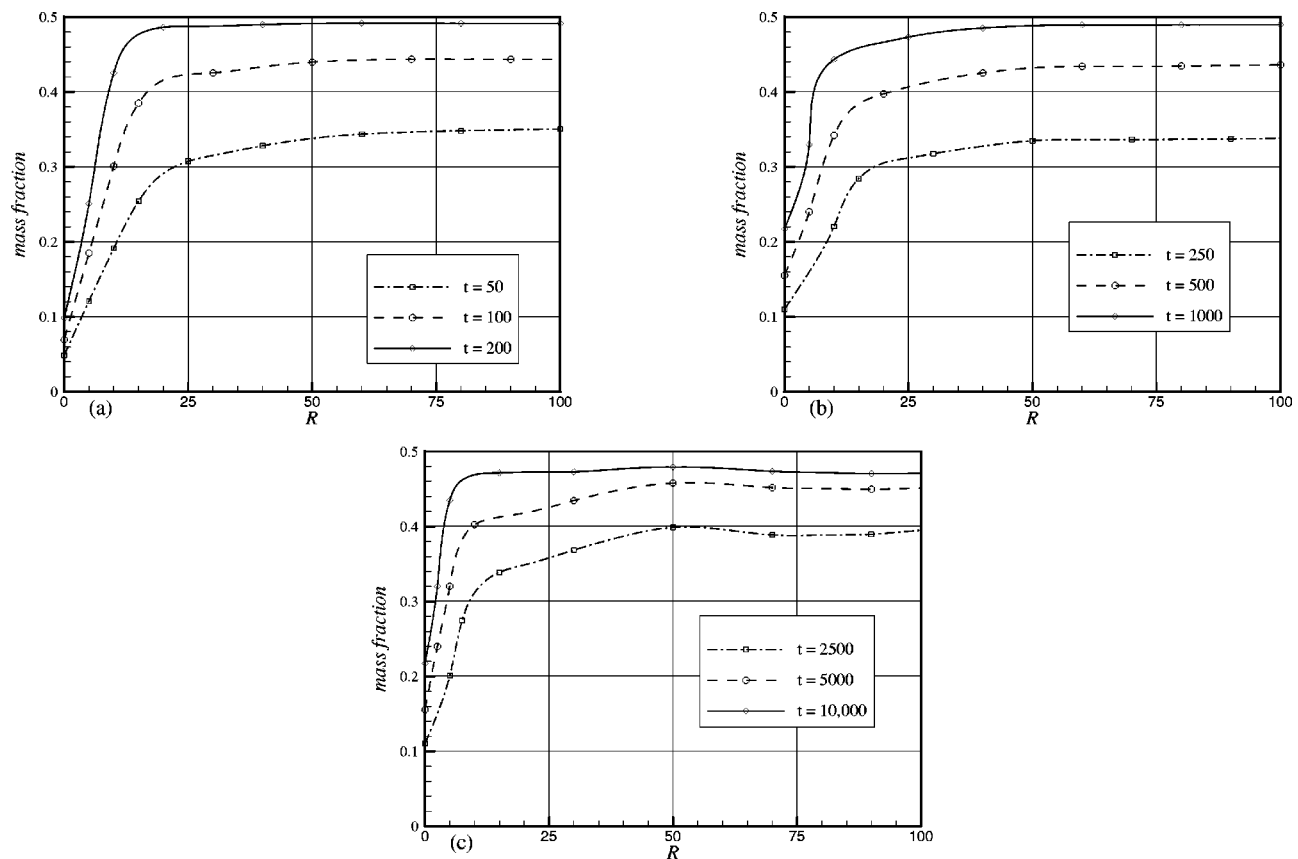
FIG. 18. Volume fraction m_f in layer 2 vs the parameter R (or the Dean number at three different times). Countercurrent flow, $0 \leqslant R \leqslant 100$, $0 \leqslant D \leqslant 4472$, $G_{21} = -1$, $\mu_{12} = 0.96$. (a) Pe$=10^3$, (b) Pe$=10^4$, (c) Pe$=10^5$.

dimensionless curvature of the pipe ε on the flow field and the mass transfer rate was studied in the present work for two-layer flows in the range of $\varepsilon = 0.01 - 0.1$. Some additional numerical and experimental results on the effect of ε on single-layer fluid flows at the values of ε as high as 0.317 can be found in Ref. 7. Both works, however, fully dispense with the possible torsion of the pipe axis, which might limit application of the present results to helical pipes. A recently published Ref. 25 and references therein shed some light on the effect of torsion on the transverse flow field in single-fluid flows. The numerical and experimental results of the latter work show that as pipe torsion increases at a constant Dean number, the structure of the transverse flow changes from two counterrotating vortices to a single-vortex type. Similar results for two-fluid flows are unavailable, and the present group has undertaken such calculations, which will be reported separately. It is clear that a transition from a two-vortex secondary flow to a single-vortex type will reduce efficiency of the method of enhancement of the interfacial mass transfer discussed in the present work. Therefore there should exist a limitation on the value of the dimensionless pipe torsion, which guarantees a two-vortex structure of the secondary flow and the enhanced interfacial mass transfer.

IV. CONCLUSIONS

Two-liquid flows in a coiled circular pipe with vanishing torsion and their effect on the mass transfer through the liquid–liquid interface are studied. Patterns of the Dean vortices appearing in the transverse flow are reported. In particular, it is shown that the flow along the immiscible liquid–liquid interface is in opposite directions in the cases of cocurrent and countercurrent axial flow. In the countercurrent case the Dean vortices are found to split into two vortices in each liquid layer, which leads to a certain decrease in the velocity of the transverse flow. It is also shown that the intensity of these vortices does not increase monotonically with increase of the Reynolds (or Dean) number, albeit it virtually saturates at higher values of Re (or D). This results in a similar behavior of the mass transfer rate versus the Reynolds (or Dean) number. Both the cocurrent and countercurrent cases studied lead eventually to similar enhancement of the mass transfer.

It is shown that the Dean vortex flow considered can be an effective tool for enhancement of the mass transfer through liquid–liquid interfaces, especially in cases when the Schmidt number is large (e.g., Sc$\sim 10^3$, as for proteins). It is emphasized that the Dean vortices provide a stronger mixing mechanism than the Taylor–Couette counterparts. It is also emphasized that such a coiled-pipe-based bioseparator/bioreactor should not contain any moving boundaries and the flow inside it can be sustained for a long time. There exists an optimal value of the Reynolds (or Dean) number (optimal axial flow rate) which yields the most effective mass transfer enhancement. The optimal value was found to be about $R = 20$ (or Re$=50$ and D≈ 180), which is not very high and

Phys. Fluids, Vol. 15, No. 2, February 2003

Dean vortices-induced enhancement   345

can be easily reached in practice. No definite scaling law for the diffused mass fraction versus the Reynolds, Dean, or Peclet numbers was found.

ACKNOWLEDGMENTS

APPENDIX A: CONTINUITY, MOMENTUM, AND MASS TRANSFER EQUATIONS IN HELICAL COORDINATES (r, θ, s)

The Lamé coefficients of the coordinate system shown in Fig. 1 are

$$h_r = 1, \quad h_\theta = r, \quad h_s = 1 + \varepsilon r \sin \theta. \tag{A1}$$

The corresponding equations can be derived from their counterparts in general orthogonal curvilinear coordinates (see, for example Ref. 17). Assuming $\partial/\partial s \equiv 0$, the continuity equation reads

$$\frac{\partial}{\partial r}[r(1+\varepsilon r \sin \theta)u] + \frac{\partial}{\partial \theta}[(1+\varepsilon r \sin \theta)v] = 0; \tag{A2}$$

the r, θ, and s projections of the momentum equations are

$$\frac{\partial u}{\partial t} + u \frac{\partial u}{\partial r} + \frac{v}{r} \frac{\partial u}{\partial \theta} - \frac{v^2}{r} - \frac{\varepsilon \sin \theta}{1+\varepsilon r \sin \theta} w^2 = -\frac{\partial p}{\partial r} + \frac{1}{R}\left\{ \frac{\partial}{\partial r}\left[\frac{1}{r(1+\varepsilon r \sin \theta)} \frac{\partial}{\partial r}[r(1+\varepsilon r \sin \theta)u]\right] + \frac{1}{r^2(1+\varepsilon r \sin \theta)} \frac{\partial}{\partial \theta}\right.$$
$$\left. \times \left[(1+\varepsilon r \sin \theta) \frac{\partial u}{\partial \theta}\right] - \frac{2}{r^2}\frac{\partial v}{\partial \theta} - \varepsilon \frac{\cos \theta + \varepsilon r \sin(2\theta)}{r(1+\varepsilon r \sin \theta)^2} v - \varepsilon^2 \frac{\cos \theta}{(1+\varepsilon r \sin \theta)^3} w \right\}, \tag{A3}$$

$$\frac{\partial v}{\partial t} + u \frac{\partial v}{\partial r} + \frac{v}{r} \frac{\partial v}{\partial \theta} + \frac{uv}{r} - \frac{\varepsilon \cos \theta}{1+\varepsilon r \sin \theta} w^2$$
$$= -\frac{1}{r}\frac{\partial p}{\partial \theta} + \frac{1}{R}\left\{ \frac{1}{1+\varepsilon r \sin \theta} \frac{\partial}{\partial r}\left[\frac{1}{r}(1+\varepsilon r \sin \theta) \frac{\partial(rv)}{\partial r}\right] \right.$$
$$\left. + \frac{1}{r^2}\frac{\partial}{\partial \theta}\left[\frac{1}{1+\varepsilon r \sin \theta} \frac{\partial}{\partial \theta}[(1+\varepsilon r \sin \theta)v]\right] + \frac{2}{r^2}\frac{\partial u}{\partial \theta} + \varepsilon \frac{\cos \theta}{r(1+\varepsilon r \sin \theta)^2}u + \varepsilon^2 \frac{\varepsilon r + \sin \theta}{(1+\varepsilon r \sin \theta)^3} w \right\}, \tag{A4}$$

$$\frac{\partial w}{\partial t} + u \frac{\partial w}{\partial r} + \frac{v}{r} \frac{\partial w}{\partial \theta} + \frac{\varepsilon \sin \theta}{1+\varepsilon r \sin \theta} uw + \frac{\varepsilon \cos \theta}{1+\varepsilon r \sin \theta} vw$$
$$= -G_i + \frac{1}{R}\left\{ \frac{1}{r}\frac{\partial}{\partial r}\left[\frac{r}{1+\varepsilon r \sin \theta} \frac{\partial}{\partial r}[(1+\varepsilon r \sin \theta)w]\right] \right.$$
$$+ \frac{1}{r^2}\frac{\partial}{\partial \theta}\left[\frac{1}{1+\varepsilon r \sin \theta} \frac{\partial}{\partial \theta}[(1+\varepsilon r \sin \theta)w]\right]$$
$$\left. + \varepsilon^2 \frac{\cos \theta}{(1+\varepsilon r \sin \theta)^3}u - \varepsilon^2 \frac{\varepsilon r + \sin \theta}{(1+\varepsilon r \sin \theta)^3}v \right\}, \tag{A5}$$

where $G_i = 1$ or G_{21} for liquids 1 and 2, respectively.

Note that $\mathrm{Re} = R^2/8$, and $D = 8(2\varepsilon)^{1/2}\,\mathrm{Re} = (2\varepsilon)^{1/2}R^2$.

The mass transfer equation is

$$\frac{\partial c}{\partial t} + u \frac{\partial c}{\partial r} + \frac{v}{r} \frac{\partial c}{\partial \theta}$$
$$= \frac{1}{\mathrm{Pe}}\left\{ \frac{1}{r}\frac{\partial(rc)}{\partial r} + \frac{1}{r^2}\frac{\partial^2 c}{\partial \theta^2} + \frac{\varepsilon \sin \theta}{1+\varepsilon r \sin \theta} \frac{\partial c}{\partial r} \right.$$
$$\left. + \frac{\varepsilon \cos \theta}{1+\varepsilon r \sin \theta} \frac{1}{r}\frac{\partial c}{\partial \theta} \right\}. \tag{A6}$$

The stream function ψ of the transverse flow is given by

$$u = \frac{1}{r(1+\varepsilon r \sin \theta)} \frac{\partial \psi}{\partial \theta}, \quad v = -\frac{1}{1+\varepsilon r \sin \theta} \frac{\partial \psi}{\partial r}, \tag{A7}$$

and is rendered dimensionless by $(G_1 a^3/\rho_1)^{1/2}$.

APPENDIX B: ANALYTICAL SOLUTION FOR THE FLOW FIELD IN A SINGLE-LIQUID CASE FOR SMALL CURVATURE

To derive the analytical solution for small curvature we assume that the axial velocity is of order 1 and the transverse flow of order ε. Thus, separating all the terms of order 1 in Eq. (A5) and all those of order ε in Eqs. (A2)–(A4), we arrive at the following equations.

The continuity equation

$$\frac{1}{r}\frac{\partial(ru)}{\partial r} + \frac{1}{r}\frac{\partial v}{\partial \theta} = 0, \tag{B1}$$

and the momentum equations

$$-\frac{\partial p}{\partial r} + \frac{1}{R}\left\{ \frac{\partial}{\partial r}\left[\frac{1}{r}\frac{\partial(ru)}{\partial r}\right] + \frac{1}{r^2}\frac{\partial^2 u}{\partial \theta^2} - \frac{2}{r^2}\frac{\partial v}{\partial \theta} \right\} = -\varepsilon w^2 \sin \theta, \tag{B2}$$

$$-\frac{1}{r}\frac{\partial p}{\partial \theta}+\frac{1}{R}\left\{\frac{\partial}{\partial r}\left[\frac{1}{r}\frac{\partial(rv)}{\partial r}\right]+\frac{1}{r^2}\frac{\partial^2 v}{\partial \theta^2}+\frac{2}{r^2}\frac{\partial u}{\partial \theta}\right\}$$

$$=-\varepsilon w^2 \cos\theta, \tag{B3}$$

$$-1+\frac{1}{R}\frac{1}{r}\frac{d}{dr}\left[r\frac{dw}{dr}\right]=0. \tag{B4}$$

Equations (B1)–(B4) must be solved with the no-slip boundary condition at $r=1$. The solution is[13,16]

$$w=\frac{R}{4}(1-r^2), \tag{B5}$$

$$u=\varepsilon\frac{R^3}{1152}\left(1-\frac{r^2}{4}\right)(1-r^2)^2\sin\theta, \tag{B6}$$

$$v=-\varepsilon\frac{R^3}{4608}(r^2-1)(7r^4-23r^2+4)\cos\theta, \tag{B7}$$

$$p=\varepsilon\frac{R^2}{192}r(2r^4-6r^2+9)\sin\theta. \tag{B8}$$

This solution corresponds to small values of the Dean number $D=8(2\varepsilon)^{1/2}\mathrm{Re}=(2\varepsilon)^{1/2}R^2$. The dimensionless stream function of the flow ψ is given by (A7), (B6), and (B7) in this limit ($\varepsilon\to 0$) as per

$$\psi=-\varepsilon\frac{R^3}{1152}r\left(1-\frac{r^2}{4}\right)(1-r^2)^2\cos\theta, \tag{B9}$$

where it is rendered dimensionless by $(G_1 a^3/\rho_1)^{1/2}$.

APPENDIX C: CALCULATION OF THE SHERWOOD NUMBER WITHIN THE FRAMEWORK OF THE BOUNDARY LAYER MODEL

We assume that the admixture concentration varies only in a thin boundary layer near the interface in both liquids 1 and 2, which is a plausible approximation based on the fact that $\mathrm{Sc}\gg 1$. In the present case $c_k=c_k(r,\theta)$ and the dimensionless Eqs. (9) and (10) in the boundary layer approximation take the form

$$\varepsilon U_k\frac{\partial c_k}{\partial r}+\varepsilon\frac{V_k}{r}\frac{\partial c_k}{\partial \theta}=\frac{1}{\mathrm{Pe}_k}\frac{1}{r^2}\frac{\partial^2 c_k}{\partial \theta^2}, \tag{C1}$$

where $\varepsilon U_k=u_k$ and $\varepsilon V_k=v_k$ are the u and v velocity components in the kth layer, respectively, and Pe_k are the Peclet numbers defined as $\mathrm{Pe}_k=\bar{W}_1 a_1/D_k$. In the present case we assume $\rho_{21}=\mu_{21}=1$, as well as $G_{21}=1$. As a result, $U_1=U_2=U$ and $V_1=V_2=V$. According to Eqs. (B6), (B7), and (B9),

$$U=\frac{A(r)}{r}\sin\theta, \tag{C2}$$

$$V=\frac{dA}{dr}\cos\theta, \tag{C3}$$

$$A(r)=\frac{\mathrm{Re}}{18}r\left(1-\frac{r^2}{4}\right)(1-r^2)^2. \tag{C4}$$

At the interface $\theta=\mp\pi/2$, Eq. (C1) takes the form

$$\varepsilon\mathrm{Pe}_k\left(-\frac{A}{r}\frac{\partial c_k}{\partial x}\pm\frac{dA/dr}{r}y\frac{\partial c_k}{\partial y}\right)=\frac{\partial^2 c_k}{\partial y^2}, \tag{C5}$$

where Eqs. (C2) and (C3) were used and the coordinate y is normal to x (normal to the interface; the coordinates are dimensionless). Since at the interface $\theta=\mp\pi/2$ we have $x=\pm r$, and Eq. (C5) can be rearranged to the following form:

$$\frac{\partial^2 c_k}{\partial y^2}+P_k(x)y\frac{\partial c_k}{\partial y}=Q_k(x)\frac{\partial c_k}{\partial x}, \tag{C6}$$

where

$$\left.\begin{array}{l}P_k=\varepsilon\mathrm{Pe}_k\left(\mp\dfrac{dA/dr}{r}\right)\\[12pt]Q_k=-\varepsilon\mathrm{Pe}_k\dfrac{A}{r}\end{array}\right\}\quad\text{at}\quad\theta=\mp\pi/2. \tag{C7}$$

Solution of Eq. (C6) is subject to the following boundary conditions:

$$y=-\infty,\quad c_2=c_{\infty 2}, \tag{C8}$$

$$y=+\infty,\quad c_1=c_{\infty 1}, \tag{C9}$$

$$y=0,\quad -D_2\frac{\partial c_2}{\partial y}=-D_1\frac{\partial c_1}{\partial y}, \tag{C10}$$

$$y=0,\quad c_1=c_2, \tag{C11}$$

and solution of the problem (C6)–(C11) yields[4]

$$c_2=\frac{c_{\infty 2}+\kappa c_{\infty 1}}{1+\kappa}-\frac{\kappa(c_{\infty 2}-c_{\infty 1})}{1+\kappa}\mathrm{erf}\left(\frac{Z}{2}\right), \tag{C12}$$

$$c_1=\frac{c_{\infty 2}+\kappa c_{\infty 1}}{1+\kappa}-\frac{(c_{\infty 2}-c_{\infty 1})}{1+\kappa}\mathrm{erf}\left(\frac{Z}{2}\right), \tag{C13}$$

where

$$\kappa=D_{21}^{-1/2}, \tag{C14}$$

$$Z=y\left[\int_1^x\frac{e^{W(\xi)-W(x)}}{Q_k(\xi)}d\xi\right]^{1/2}, \tag{C15}$$

$$W(x)=2\int_{\mathrm{const}}^x\frac{P_k(\xi)}{Q_k(\xi)}d\xi. \tag{C16}$$

Given Eqs. (C4), (C7), and (C16), we find

$$W(\xi)-W(x)=2\ln\left[\frac{\xi(1-\xi^2/4)(1-\xi^2)^2}{x(1-x^2/4)(1-x^2)^2}\right] \tag{C17}$$

for $\theta=\mp\pi/2$.

Therefore the mass flux $j_2=-(D_2/a)\partial c_2/\partial y|_{y=0}$ is found from (C12), (C15), and (C17) as

$$j_2=\frac{D_2}{a\sqrt{\pi}}\frac{\kappa(c_{\infty 2}-c_{\infty 1})}{1+\kappa}$$

$$\times\left[\frac{\varepsilon\mathrm{Pe}_2(\mathrm{Re}/18)x^2(1-x^2/4)^2(1-x^2)^4}{22/315-x^3/3+9x^5/20-3x^7/14+x^9/36}\right]^{1/2}. \tag{C18}$$

Obviously, $j_1=j_2$. The Sherwood number is defined as

$$\mathrm{Sh}_{\mathrm{BL}}(x) = \frac{j_2 a}{(c_{\infty 2} - c_{\infty 1})D_2}, \tag{C19}$$

which yields, with the aid of Eq. (C18), the expressions (18) and (19).

[1] G. Baier, T. M. Grateful, M. D. Graham, and E. N. Lightfoot, "Prediction of mass transfer rates in spatially periodic flows," Chem. Eng. Sci. **54**, 343 (1999).

[2] G. Baier, M. D. Graham, and E. N. Lightfoot, "Mass transport in a novel two-fluid vortex extractor," AIChE J. **46**, 2395 (2000).

[3] A. L. Yarin, A. Yu. Gelfgat, and P. Z. Bar-Yoseph, "Enhancement of mass transfer in a two-layer Taylor–Couette apparatus with axial flow," Int. J. Heat Mass Transf. **45**, 555 (2002).

[4] A. L. Yarin, "Stationary d.c. streaming due to shape oscillations of a droplet and its effect on mass transfer in liquid–liquid interfaces," J. Fluid Mech. **444**, 321 (2001).

[5] A. L. Yarin, "Steady streaming and mass transfer due to capillary waves in a two-layer system," Fluid Dyn. Res. **31**, 79 (2002).

[6] K. Y. Chung, M. E. Brewster, and G. Belfort, "Dean vortices with wall flux in a curved channel membrane system. 3. Concentration polarization in a spiral reverse osmosis slit," J. Chem. Eng. Jpn. **31**, 683 (1998).

[7] H. Mullubhotla, G. Belfort, W. A. Edelstein, and T. A. Early, "Dean vortex stability using magnetic resonance flow imaging and numerical analysis," AIChE J. **47**, 1126 (2001).

[8] J. J. Sillekens, C. C. M. Rindt, and A. A. van Steenhoven, "Developing mixed convection in a coiled heat exchanger," Int. J. Heat Mass Transf. **41**, 61 (1998).

[9] N. Acharya, M. Sen, and H.-C. Chang, "Analysis of heat transfer enhancement in coiled-tube heat exchangers," Int. J. Heat Mass Transf. **44**, 3189 (2001).

[10] S. Lugue, H. Mallubhotla, G. Gehlert, R. Kuriel, S. Dzengeleski, S. Pearl, and G. Belfort, "A new coiled hollow-fiber module for enhanced microfiltration performance in biotechnology," Biotechnol. Bioeng. **65**, 247 (1999).

[11] T. Kluge, C. Rezende, D. Wood, and G. Belfort, "Protein transmission during Dean vortex microfiltration of yeast suspensions," Biotechnol. Bioeng. **65**, 649 (1999).

[12] S. A. Berger and L. Talbot, "Flow in curved pipes," Annu. Rev. Fluid Mech. **15**, 461 (1983).

[13] T. J. Pedley, *Fluid Mechanics of Large Blood Vessels* (Cambridge University Press, Cambridge, 1980).

[14] W. R. Dean, "Fluid in a curved channel," Proc. R. Soc. London, Ser. A **121**, 402 (1928).

[15] A. Yu. Gelfgat, A. L. Yarin, and P. Z. Bar-Yoseph, "Three-dimensional instability of a two-layer Dean flow," Phys. Fluids **13**, 3185 (2001).

[16] W. R. Dean, "The stream-line motion of fluid in a curved pipe," Philos. Mag. **5**, 673 (1928).

[17] M. Germano, "On the effect of torsion on a helical pipe flow," J. Fluid Mech. **125**, 1 (1982).

[18] L. Zabielski and A. J. Mestel, "Steady flow in a helically symmetric pipe," J. Fluid Mech. **370**, 297 (1998).

[19] T. Hüttl, C. Wagner, and R. Friedrich, "Navier-Stokes solutions of laminar flows based on orthogonal helical coordinates," Int. J. Numer. Methods Fluids **29**, 749 (1999).

[20] Y. Fan, R. I. Tanner, and N. Phan-Thien, "Fully developed viscous and viscoelastic flows in curved pipes," J. Fluid Mech. **44**, 327 (2001).

[21] A. Yu. Gelfgat, P. Z. Bar-Yoseph, and A. Solan, "Vortex breakdown and instability of swirling flow in a cylinder with rotating top and bottom," Phys. Fluids **8**, 2614 (1996).

[22] W. M. Collins and S. C. R. Dennis, "The steady motion of viscous fluid in a curved tube," Q. J. Mech. Appl. Math. **28**, 133 (1975).

[23] D. J. McConalogue and R. S. Srivastava, "Motion of fluid in a curved tube," Proc. R. Soc. London, Ser. A **307**, 37 (1968).

[24] P. B. Rhines and W. R. Young, "How rapidly is a passive scalar mixed within closed streamlines?" J. Fluid Mech. **133**, 133 (1983).

[25] K. Yamamoto, A. Aribowo, Y. Hayamizu, T. Hirose, and K. Kawahara, "Visualization of the flow in a helical pipe," Fluid Dyn. Res. **30**, 251 (2002).